

The Fires, Asian, and Stratospheric Transport-Las Vegas Ozone Study (*FAST-LVOS*)

Andrew O. Langford¹, Christoph J. Senff^{1,2}, Raul J. Alvarez II¹, Ken C. Aikin^{1,2}, Sunil Baidar^{1,2},
Timothy A. Bonin^{1,2*}, W. Alan Brewer¹, Jerome Brioude³, Steven S. Brown^{1,4}, Joel D. Burley⁵, Dani J.
5 Caputi⁶, Stephen A. Conley⁷, Patrick D. Cullis^{2,8}, Zachary C. J. Decker^{1,2}, Stéphanie Evan³, Guillaume
Kirgis^{1,2§}, Meiyun Lin^{9,10}, Mariusz Pagowski^{2,11}, Jeff Peischl^{1,2}, Irina Petropavlovskikh^{2,8}, R. Bradley
Pierce¹², Thomas B. Ryerson^{1,7}, Scott P. Sandberg¹, Chance W. Sterling^{2,8¶}, Ann M. Weickmann^{1,2}, Li
Zhang^{9,10†}

¹NOAA Chemical Sciences Laboratory, Boulder, CO, USA.

10 ²Cooperative Institute for Research in Environmental Sciences, University of Colorado, Boulder, CO, USA.

³Laboratoire de l'Atmosphère et des Cyclones (LACy), UMR 8105, CNRS, Université de La Réunion, Météo-France, Saint-Denis, La Reunion, France.

⁴Department of Chemistry, University of Colorado, Boulder, CO, USA.

⁵Department of Chemistry, St. Mary's College of California, Moraga, CA, USA.

15 ⁶Department of Land, Air, and Water Resources, University of California, Davis, CA, USA.

⁷Scientific Aviation, Inc., Boulder, Colorado, USA.

⁸NOAA Global Monitoring Laboratory, Boulder, CO, USA.

⁹Program in Atmospheric and Oceanic Sciences, Princeton University, NJ, USA.

¹⁰NOAA Geophysical Fluid Dynamics Laboratory, Princeton, NJ, USA.

20 ¹¹NOAA Global Systems Laboratory, Boulder, CO, USA.

¹²NOAA/NESDIS Center for Satellite Applications and Research, Cooperative Institute for Meteorological Satellite Studies, Madison, WI, USA.

* Now at: MIT Lincoln Laboratory, Lexington MA, USA.

25 § Now at: 2210 Kirby Ave, Chattanooga, TN, USA.

¶ Now at: C&D Technologies Inc., Philadelphia, PA, USA.

† Now at: Department of Meteorology and Atmospheric Science, The Pennsylvania State University, University Park, PA, USA

Correspondence to: Andrew O. Langford (andrew.o.langford@noaa.gov)

30

Abstract.

The *Fires, Asian, and Stratospheric Transport-Las Vegas Ozone Study (FAST-LVOS)* was conducted in May and June of 2017 to study the transport of ozone (O_3) to Clark County, Nevada, a marginal non-attainment area in the Southwestern United States. This 6-week (20 May-30 June 2017) field campaign used lidar, ozonesonde, aircraft, and in-situ measurements in conjunction with a variety of models to characterize the distribution of O_3 and related species above southern Nevada and neighboring California, and to probe the influence of stratospheric intrusions, wildfires, and local, regional, and Asian pollution on surface O_3 concentrations in the Las Vegas Valley (≈ 900 m above sea level, a.s.l.). In this paper, we describe the *FAST-LVOS* campaign and present case studies illustrating the influence of different transport processes on background O_3 in Clark County and southern Nevada. The companion paper by Zhang et al. (2020) describes the use of the AM4 and GEOS-Chem global models to simulate the measurements and estimate the impacts of transported O_3 on surface air quality across the greater Southwestern U.S. and Intermountain West. The *FAST-LVOS* measurements found elevated O_3 layers above Las Vegas on more than 75% (35 of 45) of the sample days, and show that entrainment of these layers contributed to mean 8-h average regional background O_3 concentrations of 50-55 parts-per-billion by volume (ppbv) or about $85\text{-}95\text{ }\mu\text{g m}^{-3}$. These high background concentrations constitute 70-80% of the current U.S. National Ambient Air Quality Standard (NAAQS) of 70 ppbv ($\approx 120\text{ }\mu\text{g m}^{-3}$ at 900 m a.s.l.) for the daily maximum 8-h average (MDA8), and will make attainment of the more stringent standards of 60 or 65 ppbv currently being considered extremely difficult in the interior SWUS.

50 1 Introduction

Ground-level ozone (O_3) is one of six “criteria” air pollutants identified as serious threats to human health and welfare and made subject to National Ambient Air Quality Standards (NAAQS) by the U.S. Clean Air Act (CAA) (Karstadt et al., 1993). Ozone is not directly emitted into the atmosphere by anthropogenic activities, but is a secondary product of photochemical reactions between nitrogen oxides (NO_x = nitric oxide (NO) + nitrogen dioxide (NO_2)), and carbon monoxide (CO), methane (CH_4), or volatile organic compounds (VOCs). Thus, efforts to control ambient O_3 concentrations have sought to reduce anthropogenic emissions of these precursors, and more stringent NO_x emission controls have contributed to a 36% decrease in the annual mean daily maximum 1-h NO_2 , the benchmark used to ascertain NAAQS attainment, across the U.S. between 55 2000 and 2019 (<https://www.epa.gov/air-trends/nitrogen-dioxide-trends>, last access 16 August 2021). In response, the U.S. mean 4th highest annual maximum daily 8-h average (4MDA8) O_3 , the metric by which compliance with the O_3 NAAQS is 60 determined, declined from 82 to 65 parts-per-billion by volume (ppbv) or 21% over the same period (<https://www.epa.gov/air-trends/ozone-trends>, last access 16 August 2021).

The air quality improvements in the U.S. over the last two decades represent a major success, but the gains have not been uniform, with large decreases in the Southeast U.S. (SEUS: Alabama, Florida, Georgia, North Carolina, South Carolina, and 65 Virginia) where NO_2 and O_3 declined by 39 and 25%, respectively, but much smaller changes in the Southwest U.S. (SWUS: Utah, Arizona, Colorado, and New Mexico) where a 38% reduction in NO_2 led to an O_3 decline of just 11%. The 4MDA8 O_3 decreased from 83 to 63 ppbv in the SEUS, but only decreased from 77 to 69 ppbv in the SWUS. The weaker response to 70 NO_2 reductions in the SWUS is attributed in part to increased oil and gas development (Pozzer et al., 2020) and in part to the much higher background O_3 in this region (EPA, 2013; Lefohn et al., 2014; Cooper et al., 2015). This background is derived 75 from a variety of non-controllable ozone sources (NCOS) including O_3 produced by photochemical reactions of anthropogenic emissions outside the U.S. borders, or by soils, vegetation, lightning, or wildfires, and by naturally-occurring O_3 transported downward from the stratosphere (Jaffe et al., 2018). The high mean elevations of Colorado (2078 m a.s.l.), Wyoming (2047 m a.s.l.), Utah (1864 m a.s.l.), Nevada (1681 m a.s.l.), and Idaho (1528 m a.s.l.), which make up the heart of the Intermountain West (IMW), i.e., the area of the U.S. bounded by the Cascade (≤ 4392 m a.s.l.) and Sierra Nevada (≤ 4421 80 m a.s.l.) Mountains to the west and the Front Range of the Rocky Mountains (≤ 4401 m a.s.l.) to the east (Fig. 1a), make this entire region particularly vulnerable to both stratospheric intrusions (Lin et al., 2012a) and pollution transported across the Pacific Ocean from East Asia (Lin et al., 2012b).

Background O_3 cannot be directly measured, but an upper limit can be estimated from measurements at remote “baseline” 85 locations sufficiently removed from anthropogenic sources. Jaffe et al. (2018) estimated that the monthly mean MDA8 O_3 in the higher elevations of the IMW is around 50 ppbv in late spring with the 4MDA8 O_3 concentrations exceeding 60 ppbv in some locations. These high baseline concentrations constitute more than 70% of the 70 ppbv NAAQS set in 2015 (EPA, 2014) and limit the ability of western air quality managers to maintain surface O_3 concentrations below this standard through local control strategies (Cooper et al., 2015; Uhl and Moore, 2018; Faloona et al., 2020).

Concern about the potential impacts of stratospheric intrusions, Asian pollution, and other non-controllable ozone sources (NCOS) on NAAQS attainment in the greater Las Vegas area motivated the first Las Vegas Ozone Study (LVOS) conducted by the NOAA Chemical Sciences Laboratory (CSL) in late May and June of 2013 (Langford et al., 2015b) in partnership with the Clark County (Nevada) Department of Air Quality (CCDAQ). The LVOS 2013 field campaign was organized 90 around the truck-mounted TOPAZ (Tunable Optical Profiler for Aerosol and oZone) differential absorption lidar (Alvarez II et al., 2008) which is part of the NASA-sponsored Tropospheric Ozone Network (TOLNet). The lidar was deployed for 6 weeks to a decommissioned U.S. Air Force radar base on the summit of Angel Peak (AP: 36.32 °N, -115.57 °E, 2680 m above mean sea level, a.s.l.) about 45 km west of Las Vegas in the Spring Mountains (Fig. 1c). The lidar measurements were augmented by *in-situ* measurements of O_3 and CO and basic meteorological parameters.

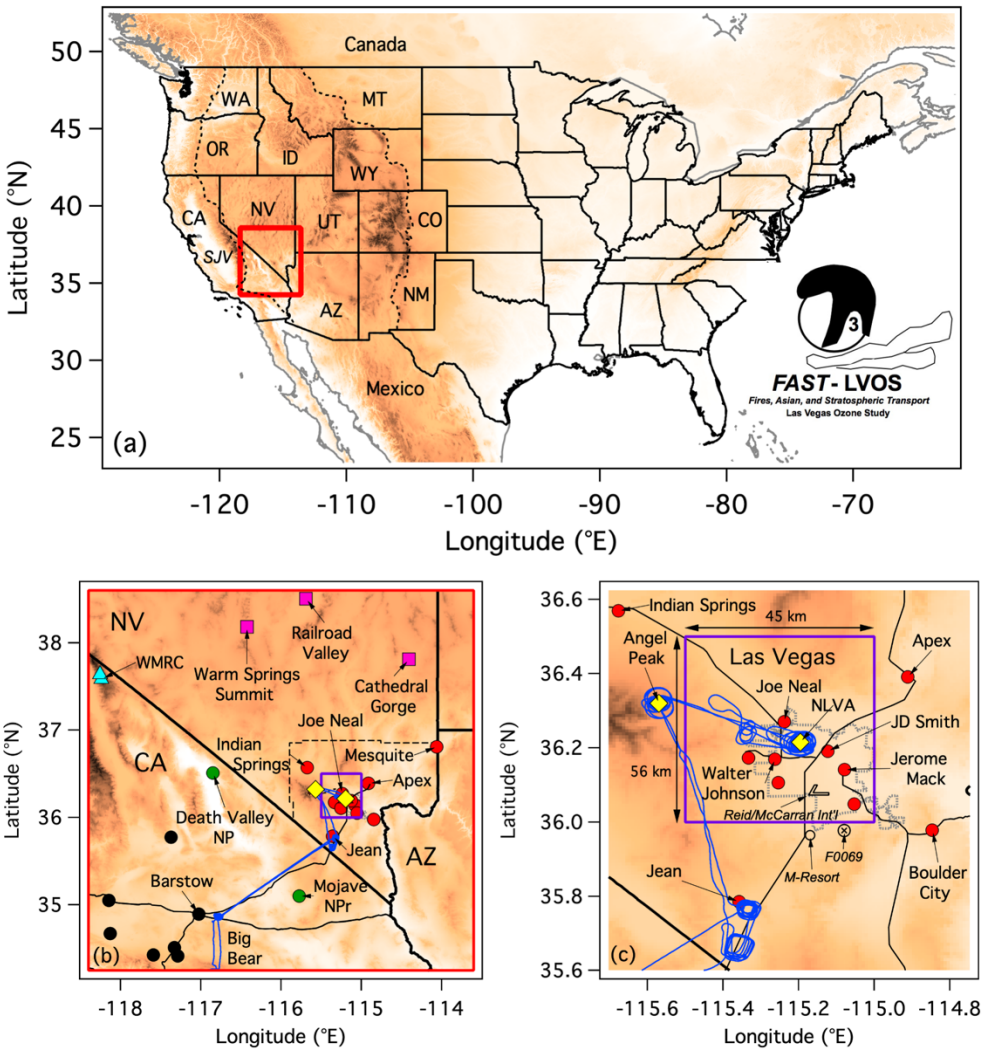


Figure 1: (a) Shaded relief map of the contiguous U.S. showing the FAST-LVOS study domain (red box). The dashed black line outlines the U.S. Intermountain West. The San Joaquin Valley (SJV) was studied the previous summer in the CABOTS field campaign. (b) and (c), Expanded views of the study area. The solid and dashed black lines in (b) mark the state and Clark County borders, respectively. The dotted black line in (c) outlines the Las Vegas metropolitan area. The color filled circles mark regulatory O₃ monitors maintained by Clark County (red), the US National Park Service (green), and the California Air Resources Board (black). The magenta squares and cyan triangles show baseline monitors operated by the Nevada Department of Environmental Quality and White Mountain Research Center, respectively. The yellow diamonds show the locations of AP and the NLVA (see text). The blue traces show the 28 June SA flight track, and the violet boxes outline the 0.25° x 0.25° (≈ 45 km H x 56 km W) FLEXPART receptor domain.

The LVOS 2013 campaign documented several episodes in which the appearance of stratospheric intrusions, Asian pollution, or wildfire plumes at AP was followed by MDA8 O₃ concentrations greater than 70 ppbv at multiple regulatory monitors in Clark County, and in some cases, by exceedances of the 2008 O₃ NAAQS of 75 ppbv then in effect. Since 110 stratospheric intrusions do not typically reach the relatively low elevations of Las Vegas (620 m a.s.l.) it was hypothesized that some of the high O₃ episodes resulted from entrainment of mid-tropospheric O₃ layers (Langford et al., 2017) by the deep convective boundary layers that form over the Mojave Desert (Seidel et al., 2012). This hypothesis could not be confirmed, however, because of the placement of the lidar above the valley floor and a more extensive follow up study, the 115 *Fires, Asian, and Stratospheric Transport-Las Vegas Ozone Study (FAST-LVOS)*, was conducted over the same time period in 2017 to: i) test the entrainment hypothesis, ii) determine the representativeness of the LVOS 2013 results, and iii) better characterize the different sources of surface O₃ in the Las Vegas Valley (LVV). In this paper, we present an overview of the 120 FAST-LVOS campaign with brief examples highlighting the influence of stratospheric intrusions, Asian pollution, biomass burning, and both local and regional pollution on surface O₃ in Clark County and the greater IMW. The companion paper by Zhang et al. (2020) uses the GFDL-AM4 and GEOS-Chem global models to simulate these measurements and quantify the impacts of these processes on high-O₃ events in southern Nevada and the greater SWUS and IMW.

2 Background

Previous airborne and ground-based lidar measurements have shown that elevated O₃ layers are common features of the lower free troposphere between \approx 3 and 6 km a.s.l. above California (Langford et al., 2012; Ryerson et al., 2013; Faloona et al., 2020) and southern Nevada (Langford et al., 2015b; 2017) in late spring and early summer, and it is well established that 125 the U.S. West Coast is one of the global hotspots for deep stratosphere-to-troposphere transport (STT) of O₃ in springtime (Wernli and Bourqui, 2002; Sprenger and Wernli, 2003; James et al., 2003; Skerlak et al., 2014; 2015; Breeden et al., 2021). This occurs primarily through the formation of tropopause folds, tongues of lower stratospheric air that descend isentropically beneath the jet stream circulating around upper-level lows. These intrusions of dry, O₃-rich air often form near 130 the end of the North Pacific storm track and descend behind the mixture of clean or polluted tropospheric air in the dry airstream (Wernli, 1997; Cooper et al., 2004; Trickl et al., 2014). They are thus an important mechanism for transport of East Asian pollution from the upper troposphere down to the boundary layer above the western U.S. (Brown-Steiner and Hess, 2011; Lin et al., 2012a; 2012b).

Tropopause folds typically follow one of two pathways as they reach the middle troposphere. Many intrusions, particularly 135 those formed by deep closed lows, continue to curve cyclonically as they descend and wrap up above the surface low in the lower troposphere (Danielsen, 1964). These deep LC2 (*lifecycle* 2) intrusions (Thorncroft et al., 1993; Polvani and Esler, 2007) often reach the top of the boundary layer and sometimes even the surface at higher elevations (Schuepbach et al., 1999; Stohl et al., 2000; Bonasoni et al., 2000; Trickl et al., 2021). These intrusions were first described by Reed and

140 *Danielsen* (Reed and Danielsen, 1958) and have long been observed as steeply sloping tongues in ozone lidar curtains (Browell et al., 1987; Ancellet et al., 1994; Vaughan et al., 1994; Langford et al., 1996; Eisele et al., 1999).

145 Much less attention has been paid to the so-called LC1 (*lifecycle 1*) intrusions that are sheared anticyclonically from elongated troughs to form quasi-horizontal filaments in the middle and upper troposphere (Appenzeller and Davies, 1992; Appenzeller et al., 1996; Vaughan et al., 2001; Albers et al., 2021). These *streamers* are well known features of satellite water vapor imagery (Manney and Stanford, 1987) and can stretch for thousands of kilometres. They usually roll up horizontally into a series of diminishing vortices to be irreversibly mixed into the free troposphere (Wirth et al., 1997; Vaughan and Worthington, 2000; Vaughan et al., 2001; Colette and Ancellet, 2006), but they can also be dissipated by moist convection (Langford and Reid, 1998). They are a significant source of background O₃ in the free troposphere (Albers et al., 2021), but usually remain well above the boundary layer and thus do not influence surface O₃ directly.

150

155 Both types of intrusions are most common in winter when cyclonic activity is at a maximum, but stratospheric intrusions that form in late May and early June are more likely to affect compliance with the ozone NAAQS since, i) more O₃ is available for transport from the lower stratospheric reservoir in springtime (Albers et al., 2018), ii) surface concentrations are higher because of increased photochemical production, and iii) deeper afternoon mixed layers (Seidel et al., 2012) can potentially entrain some intrusions that would otherwise pass overhead. Stratospheric influence plays an important role in driving the observed year-to-year variability in springtime ozone air quality over the western U.S. (Lin et al., 2015). The potential surface impacts of stratospheric intrusions and co-transported pollution decrease in summer after the jet stream migrates poleward into Canada and deep convection lifts pollution higher into the upper troposphere over East Asia (Hudman et al., 2004; Brown-Steiner and Hess, 2011).

160 **3 FAST-LVOS measurements and models**

165 The *FAST-LVOS* field experiment was also organized around the TOPAZ lidar which was upgraded with a new data acquisition system in 2015. This upgrade more than doubled the useful operating range of the lidar from \approx 3 to 8 km, which allowed it to reach higher altitudes than was possible during LVOS 2013, even while operating from a much lower elevation site at the North Las Vegas Airport (NLVA, 36.2°N, -115.2°E, 680 m a.s.l.) located about 8 km NW of downtown Las Vegas. NOAA CSL also brought a vertically-staring Doppler lidar to the NLVA to characterize mixing between the boundary layer and free troposphere, and a mobile laboratory with a more extensive suite of *in-situ* measurements to the summit of AP. These primary measurements were supplemented by measurements from a single-engine Mooney TLS Bravo aircraft operated by Scientific Aviation, Inc. (SA) and by ozonesondes launched by the NOAA Global Monitoring Laboratory (GML) during four 2-to-4 day intensive operating periods (IOPs) initiated when the synoptic conditions showed 170 that stratospheric intrusions or Asian pollution transport events were likely.

3.1 Primary measurements

3.1.1 NOAA CSL TOPAZ lidar

The TOPAZ truck arrived in Las Vegas on the morning of 17 May and was deployed to a secure CCDAQ enclosure on the north side of the NLVA. In addition to the lidar, the truck was equipped with an automated weather station (Airmar 150WX) and a commercial UV absorption O₃ monitor (2B Technologies model 205) that sampled air 5 m above the ground. The autonomous NOAA CSL vertically-staring 1.5 μ m micro-Doppler lidar was placed near the TOPAZ truck to measure aerosol backscatter and vertical wind variance for the estimation of boundary layer depths (Bonin et al., 2018). The two lidars were located near the CCDAQ wind profiler (Fig. 2, top) and visibility camera, and about 500 m NNW of the National Weather Service (NWS) KVGT meteorological tower.

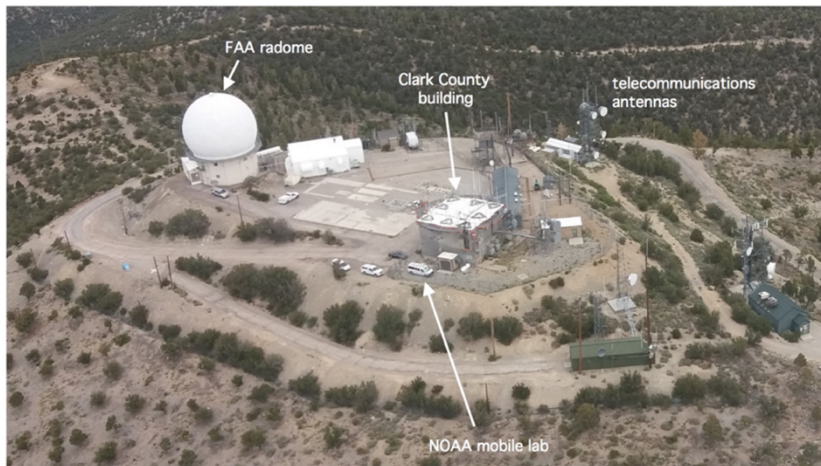
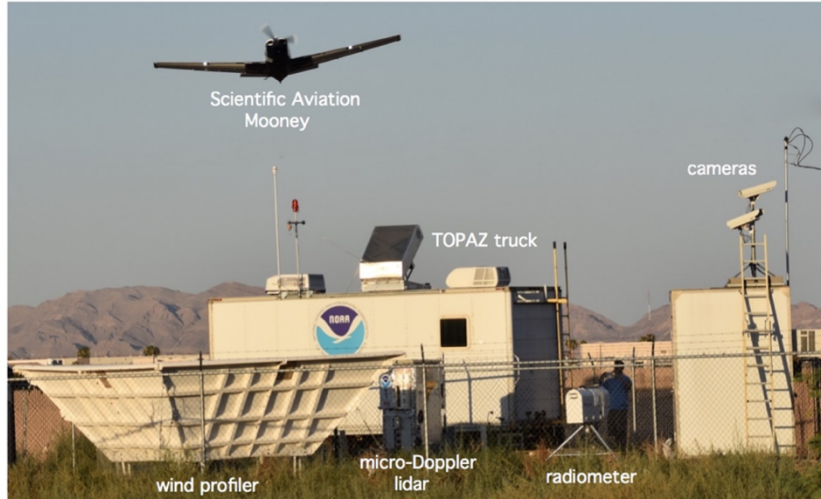
180

TOPAZ uses a tuneable Ce:LiCaF solid-state laser and a unique transceiver configuration to profile O₃ and particulate backscatter (β) from just above the surface to \approx 8 km above ground level (a.g.l.). The lidar points vertically, but uses a large steerable mirror on top of the truck to sequentially deflect the co-axial laser beams and return signals along a series of elevation angles. The scanner line of sight was oriented to the east (parallel to the 7-25 runway) and successively tilted along paths 2, 6, 20 and 90° above the horizon. This cycle was repeated every 8 minutes and the vertical projections of the slant profiles merged with the zenith profile to create vertical ozone and backscatter profiles starting 27.5 \pm 5 m above the ground with the lowest measurements displaced about 800 m downrange. Ozone number densities were retrieved using two wavelengths (\approx 287 and 294 nm) with 30-m range gates and a smoothing filter that increased from 270 m wide at the minimum range (815 ± 15 m) to 1400 m wide at the maximum range. The ozone and backscatter profiles were computed simultaneously using an iterative procedure (Alvarez II et al., 2008) incorporating the O₃ absorption cross-sections of *Malicet et al.* (Malicet et al., 1995) and temperature and pressure profiles interpolated from the 3-h National Centers for Environmental Prediction (NCEP) North American Regional Reanalysis (NARR) to account for the temperature dependence of the O₃ cross-sections and to convert the calculated O₃ number densities to mixing ratios. The effective O₃ vertical resolution increased from \approx 10 m near the surface to 150 m at 500 m a.g.l., and 900 m at 6 km a.g.l. The maximum range was limited by solar background radiation during the day and decreased from about 8 km to 6 km near midday. Backscatter from aerosols, smoke, and dust was also retrieved with 7.5 m resolution at 294 nm.

Total uncertainties in the 8-min O₃ retrievals are estimated to increase from \pm 3 ppbv below 4 km to \pm 10 ppbv at 8 km. The upgraded TOPAZ system was extensively compared with measurements from the same SA Mooney aircraft used here, as well as the NASA Alpha Jet (Hamill et al., 2016) in the 2016 CABOTS field campaign (Langford et al., 2019), and with ECC ozonesondes and ground-based TOLNet lidars in the 2016 Southern California Ozone Observation Project (SCOOP) (Leblanc et al., 2018). Both intercomparisons showed excellent agreement within the stated uncertainties of the measurement

techniques, particularly when the spatial and temporal differences introduced by the different sampling methods are considered.

205



210 **Figure 2: Photographs of the NLVA (top) and AP (bottom) FAST-LVOS ground sites. The NLVA photograph faces east and the AP photograph northwest. Note the TOPAZ scanning mirror housing near the center of the photograph with the lidar line of sight pointing away from the camera. The view of Angel Peak was taken from the SA Mooney aircraft and shows the NOAA mobile lab parked in the location occupied by the TOPAZ lidar during the 2013 LVOS campaign. Photographs by A. Langford (top) and D. Caputi (bottom).**

3.1.2 NOAA CSL Mobile Laboratory

215 The van-based CSL mobile laboratory (Wild et al., 2017) was equipped with instruments to measure O₃, CO, water vapor (H₂O), carbon dioxide (CO₂), CH₄, NO, NO₂, total reactive nitrogen oxides (NO_y), nitrous oxide (N₂O) and meteorological parameters. The NO, NO₂, NO_y, and O₃ measurements were made with a custom-built cavity-ring down spectrometer (CRDS) (Washenfelder et al., 2011; Wild et al., 2014; Womack et al., 2017), a commercial (Picarro) wavelength-scanned CRDS to measure CO₂ and CH₄ (Peischl et al., 2013), and a modified commercial (Los Gatos) instrument using off axis-
220 integrated cavity output spectroscopy (OA-ICOS) to measure N₂O, CO, and H₂O (Coggon et al., 2016). Additional details about these instruments can be found in the references. Ozone was also measured by a commercial (2B Tech, Model 205) ultraviolet photometer, and these data were used to fill in the gaps during brief periods when the CRDS instrument was offline. There were no aerosol measurements.

225 The mobile laboratory carried the same automated weather station (Airmar 150WX) as the TOPAZ truck, and was also equipped with differential GPS and sonic anemometers to measure absolute wind speed and direction while the van was moving. The laboratory was parked on the southeast edge of the AP summit overlooking Kyle Canyon, the primary corridor for upslope transport from the LVV, for most of the campaign. This is the same location (Fig. 2, bottom) occupied by the TOPAZ truck during LVOS 2013 and provides an unobstructed fetch to the west, south, and east. Northerly winds (\approx 335 and
230 65°) were perturbed by one of the nearby buildings, but winds from this direction were uncommon during the study. A few drives were conducted between AP and the LVV on 23-25 May during IOP1, and again on 15 and 17 June. These measurements will be described elsewhere. The van was also relocated to the NLVA for an intercomparison with the instruments on the SA Mooney on 15 June. All of the measurements described here are from AP.

235 The first LVOS campaign in 2013 used the relationships between the O₃, H₂O and CO measured on AP to infer the history of the air masses sampled on the summit (Langford et al., 2015b). This was made possible because of the relative remoteness and high elevation of the site, which minimized the influences of nearby NO_x or CO emissions and surface deposition, and by the lack of rainfall and extreme aridity of the Mojave Desert which makes water vapor a semi-conserved tracer. Since CO has a tropospheric lifetime of \approx 60 days and originates primarily from soil emissions and combustion processes (Holloway et
240 al., 2000), concentrations are lower in the stratosphere than in the free troposphere and terrestrial boundary layer. Conversely, O₃ concentrations are much higher in the stratosphere than in the troposphere. Thus, O₃ and CO tend to be negatively correlated in mixtures of stratospheric and free tropospheric air which is also very dry, but positively correlated in mixtures of free tropospheric air and urban pollution or biomass burning plumes. The marine boundary layer is far removed from most natural and anthropogenic sources of CO and O₃ and has low concentrations of both (Clark et al., 2015). Thus, the
245 relationships between these three parameters can be used to separate the influences of stratospheric intrusions and Asian pollution from regional pollution and wildfires, and distinguish air that descended from the lower stratosphere or upper troposphere from air advected inland from the Pacific Ocean.

This empirical approach was much improved by the addition of N₂O, NO, NO₂, NO_y, CH₄, and CO₂ measurements in the 250 2017 *FAST-LVOS* campaign. Nitrous oxide has a much longer tropospheric lifetime than CO (>100 years) and originates primarily from natural and fertilized soils (Tian et al., 2019) and the oceans (Tian et al., 2020). It is thus well-mixed throughout the free troposphere with much lower concentrations in the stratosphere, and can be used as a tracer for recent agricultural and oceanic influences and stratospheric intrusions (Hintsa et al., 1998; Assonov et al., 2013). The CH₄ 255 measurements provide another useful tracer for Asian pollution (Xiao et al., 2004), as well as oil and gas (Peischl et al., 2018), agricultural (Peischl et al., 2012), and biomass burning (Delmas, 1994) influences. The NO, NO₂, and NO_y measurements can be used to identify airmasses influenced by biomass burning or by local, regional, and Asian pollution. In particular, the short lifetime (\approx 2-4 hours) of NO_x (Laughner and Cohen, 2019) makes these measurements a useful tracer for pollution from the LVV. The CO₂ measurements can also help identify pollution and biomass burning influences, although interpretation of these measurements is complicated by the strong diurnal variations created by photosynthetic uptake.

260

3.1.3 Meteorological measurements

The temperature, pressure, relative humidity, wind speed and direction from the automated weather stations in the TOPAZ truck at the NLVA and the mobile laboratory on AP are summarized in Fig. S1. The NLVA measurements were 265 supplemented by the NWS measurements from the KVGT tower, and vertical wind information was also obtained from the radar wind profiler, ozonesondes, and aircraft. The automated micro-Doppler lidar measurements near the TOPAZ truck were used to calculate hourly averaged boundary layer heights (Bonin et al., 2018), which ranged from \approx 2 to 4 km in the afternoon. Mixed layer heights were also derived from the potential temperature and relative humidity profiles acquired by the GML ozonesondes (8 km distant), and from the afternoon (00 UT or 1700 Pacific Daylight Time, PDT) radiosondes launched from the Harry Reid (formerly McCarran) International Airport (NWS station identifier KVEF) about 15 km to the 270 south. The figure also shows solar radiation measurements from a site in Henderson near KVEF (cf. Fig. 1f) that were obtained from the University of Utah MesoWest network (<https://mesowest.utah.edu>, last access 16 August 2021) and from the Spring Mountain Youth Camp (SMYC), which occupies the former cantonment area of the decommissioned Air Force base and lies \approx 800 m west and 120 m below the AP summit. The SMYC measurements were obtained from the Western Regional Climate Center (WRCC) (www.wrcc.dri.edu/weather/smyc.html).

275

3.2 Supplemental measurements

The supplemental ozonesonde and aircraft sampling during the intensive operating periods (IOPs) provided important context for the lidar and surface measurements. The four 2-to-4 day IOPs were conducted on 23-25 May, 31 May-2 June, 10-14 June, and 27-30 June (no ozonesondes were launched on 14 and 27 June). The NOAA Global Monitoring Laboratory 280 (GML) launched a total of 30 ozonesondes (1 to 4 ozonesondes per day) from a park adjacent to the CCDAQ Joe Neal monitoring site located about 8 km northwest of the NLVA during the four IOPs. The ozonesondes (Sterling et al., 2018)

measured O₃ concentrations to altitudes well above the 8 km range of the lidar, and recorded temperature, relative humidity, and wind profiles which helped characterize the synoptic context.

285 The SA Mooney conducted daily flights between the NLVA and Big Bear, CA (cf. Fig. 1b) during the four *FAST-LVOS* IOPs, logging a total of 90 flight hours on 15 days. The aircraft carried a pilot and flight scientist, along with a 2B Technologies Model 205 O₃ monitor, an Aerodyne Research Cavity Attenuated Phase Shift (CAPS) NO₂ monitor, and a Picarro 2301f Wavelength-scanned Cavity Ring-Down Spectrometer (WS-CRDS) to measure CO₂, CH₄, ethane (C₂H₆), and H₂O (Trousdale et al., 2016). The 2B O₃ data were sampled at 2-s intervals, which corresponds to a mean distance of 150 m
290 at the typical level flight speed of 75 m s⁻¹. The standard TLS flight plan (Figs. 1b and 1c) began with a vertical profile to about 5 km a.s.l. above North Las Vegas after take-off. The aircraft then flew to AP and spiralled down around the summit to ≈3 km a.s.l. (cf. Fig. 2, bottom). From there, the aircraft headed to Jean, NV (924 m a.s.l.) where the southernmost CCDAQ O₃ monitor is located and conducted another profile. The pilot then followed the I-5 corridor before diverting south to Big Bear, CA where the aircraft landed and refuelled. The return leg began with a profile above Barstow, CA before following
295 the I-5 corridor back to Clark County with additional profiles above Jean, AP, and North Las Vegas if fuel permitted. The default flight plan was modified as necessary to account for air traffic control requirements.

3.3 Ancillary measurements

The CCDAQ maintains a network of continuous air monitoring sites (CAMS) for O₃ and other parameters (e.g., NO₂, fine
300 (PM_{2.5}) and coarse (PM₁₀) particulates, meteorology) in the LVV and surrounding areas (cf. Fig. 1). The CCDAQ also operates an upper air station consisting of a radar wind profiler and profiling radiometer at the NLVA (cf. Fig. 2, top) and automated visibility cameras at the NLVA and M-Resort (cf. Fig. 1). The CAMS network included 11 active O₃ monitors during the *FAST-LVOS* campaign with the Joe Neal (C75), Walter Johnson (C71), and JD Smith (C2002, since deactivated) monitors located within 8 km of the NLVA (cf. Fig. 1c). The hourly averaged measurements from the TOPAZ monitor at the
305 NLVA agreed with the Joe Neal and Walter Johnson measurements to within 3% on average, with linear regression coefficients of determination of R²=0.87 (NLVA-C75), R²=0.76 (NLVA-C71), and R²=0.75 (C75-C71) when the Doppler lidar showed the boundary layer was well mixed. The Joe Neal and Walter Johnson O₃ measurements are discussed in Sections 8 and 9 along with those from the more distant Apex (C22, 32 km), Jean (C1019, 49 km), Indian Springs (C7772, 58 km), and Mesquite (C23, 121 km) monitors located outside the LVV. The CCDAQ also operated a temporary O₃ monitor
310 at the SMYC; these measurements averaged ≈8% lower (R²=0.91) than both the CRDS and 2B measurements from the mobile laboratory on the summit and are not used in our analyses.

Surface O₃ measurements from other monitors operated by federal, state, local, and tribal agencies outside of Clark County were obtained from the EPA Air Quality System (AQS) (<https://www.epa.gov/aqs>, last access 16 August 2021) and Clean
315 Air Status and Trends Network (CASTNET) (<https://www.epa.gov/castnet>, last access 16 August 2021). The Nevada

Division of Environmental Protection (NVDEP) also operated 3 portable solar-powered monitors at the Warm Springs Summit (WSSU, 38.184°N, -116.425°E, 2307 m a.s.l.), Railroad Valley (RRVA, 38.504°N, -115.694°E, 1413 m a.s.l.), and Cathedral Gorge State Park (CGSP, 37.810°N, -114.410°E, 1513 a.s.l.) to measure baseline O₃ during *FAST-LVOS*. Measurements were previously made at these three sites as part of the Nevada Rural Ozone Initiative (NVROI) (Fine et al., 320 2015a; 2015b; Gustin et al., 2015). Measurements from two remote research monitors operated by the White Mountain Research Center (WMRC) (Burley and Bytnerowicz, 2011) were also shared with the *FAST-LVOS* project. The WMRC maintains the highest continuously operating surface O₃ monitors in the continental U.S. at White Mountain Summit (WMS, 37.634°N, -118.256°E, 4342 m. a.s.l.) and Barcroft Observatory (BCO, 37.590°N, -118.239°E, 3879 m a.s.l.) located ≈280 km NW of AP (cf. Fig. 1b).

325

3.4 Model support

Planning for the *FAST-LVOS* day-to-day activities and IOPs relied primarily on long range weather forecasts from the NCEP Global Forecast System (GFS) obtained from the University of Wyoming (<http://weather.uwyo.edu/models/fcst/gfs003.shtml>, last access 16 August 2021), and 4-day 1° x 1° O₃ and CO forecasts 330 from the NOAA/NESDIS RAQMS (<http://raqms-ops.ssec.wisc.edu/>, last access 16 August 2021) (Pierce et al., 2003) model. The RAQMS model also provided boundary conditions for the 13-km resolution NOAA rapid refresh RAP-Chem (<https://rapidrefresh.noaa.gov/RAPchem>, last access 15 August 2021) model. The daily forecasts from these two models were supplemented by GOES-West water vapor imagery and other satellite products obtained from the NOAA/NESDIS 335 Regional and Mesoscale Meteorology Branch (RMBB, <http://rammb.cira.colostate.edu>, last access 16 August 2021) at the Colorado State University. Data interpretation was aided by the NASA Modern-Era Retrospective-analysis for Research and 340 Applications (MERRA-2) Reanalysis (https://fluid.nccs.nasa.gov/reanalysis/classic_merra2/, last access 16 August 2021) online plotting resources (Gelaro et al., 2017), NOAA Air Resources Laboratory (ARL) HYSPLIT trajectories (Stein et al., 2015), and stratospheric, Asian pollution, and biomass burning tracers calculated with 0.25° horizontal resolution using the FLEXPART particle dispersion model driven by the European Centre for Medium-Range Weather Forecasts (ECMWF) 345 operational (0.5° x 0.5°) model (Brioude et al., 2007; 2009). The RAQMS, RAP-Chem, and FLEXPART models used in the study are described in more detail in the *FAST-LVOS* final report (<https://csl.noaa.gov/projects/fastlvos/FAST-LVOSfinalreport604318-16.pdf>, last access 7 December 2021). The *FAST-LVOS* measurements were also simulated by the GEOS-Chem (≈50 x 50 km² horizontal, 0.2 to 1.0 km vertical 350 resolution in the free troposphere) and AM4 (≈0.25° x 0.3125° horizontal, 0.1 to 1.0 km vertical resolution in the free troposphere) chemistry-climate models; these efforts are described in the companion paper by Zhang et al. (2020).

4 Meteorological contexts

The *FAST-LVOS* campaign can be divided into two meteorologically distinct periods, a late spring period from mid-May to mid-June, and an early summer period from mid-June through the end of June. The Synoptic Discussion for May 2017 from

350 the National Centers for Environmental Information (NCEI) (<https://www.ncdc.noaa.gov/sotc/synoptic/201705>, last access
16 August 2021) describes the jet stream as being very active in the late spring period with a series of closed lows and upper-
level troughs crossing the contiguous U.S. every few days. These cyclonic systems spawned a series of stratospheric
intrusions that appear as potential vorticity (PV) enhancements (Duncan et al., 2021) in the 300 hPa (≈ 9.5 km a.s.l.) NASA
MERRA-2 Reanalysis plots in Figs. 3a-3d. GOES water vapor images coinciding with the PV analyses are displayed in Fig.
355 S2. The first extratropical cyclone, designated L₁ in Fig. 3a, passed through Nevada before the official start of the campaign
on 20 May, but the next three low-pressure systems labelled L₂, L₃, and L₄ in Figs. 3b-3d were targeted by IOPs on 23-25
May, 31 May-2 June, and 11-14 June. The solar radiation data in Fig. S1 shows the appearance of cirrus ahead of the cold
fronts, as well as perturbations in the normal diurnal variations of pressure, temperature, dewpoint, and winds created by
thermally-driven regional (e.g., plains-mountain) and mesoscale (e.g., valley and slope) circulations (Stewart et al., 2002).
360 There was no measurable precipitation, but the temperatures on AP dropped below freezing on the nights of 17-18 May and
11-12 June, and the cold fronts decreased the depth of the afternoon boundary layers above the NLVA to ≈ 2 km or roughly
the elevation of AP above the valley.

365 The jet stream retreated north into Canada in the wake of L₄ and the NCEI Synoptic Discussion for June 2017 confirms that
the expanding subtropical ridge seen in Fig. 3e dominated the weather across the SWUS for the rest of the campaign
(<https://www.ncdc.noaa.gov/sotc/synoptic/201706>, last access 16 August 2021). The ridge brought clear skies, dry
conditions, and record high temperatures to Clark County, and June 2017 was the 3rd hottest in Las Vegas since official
record keeping began in 1948, and the extreme temperatures and dry conditions exacerbated multiple wildfires across the
370 SWUS. The high temperatures at the NLVA exceeded 41°C (106°F) each day during the last two weeks of the study and the
daily records for Las Vegas were tied or exceeded on 5 straight days from 20 to 24 June. The official high of 47.2°C (117°F)
at Harry Reid International Airport on 20 June, the last day of astronomical spring, tied the all-time Las Vegas record.
Coincidentally, this record was also tied on the final day of the first LVOS campaign (30 June 2013). The daily high
temperatures abated slightly to 42-43°C during the last few days of the campaign and IOP4 when a weak cold front
associated with the shallow trough (L₈) in Fig. 3f passed through the LVV. The temperatures on AP were typically 10-15°C
375 lower due to its higher elevation.

5 Overview of results

5.1 TOPAZ profiles

380 TOPAZ operated for an average of ≈ 12 hours a day over 45 consecutive days (17 May - 30 June) during *FAST-LVOS*,
accumulating a total of 4026 profiles or 537 hours of observations. Approximately 60% of the profiles were acquired
between the hours of 0900 and 1700 PDT, but there were several extended runs including a 60-hour continuous session on

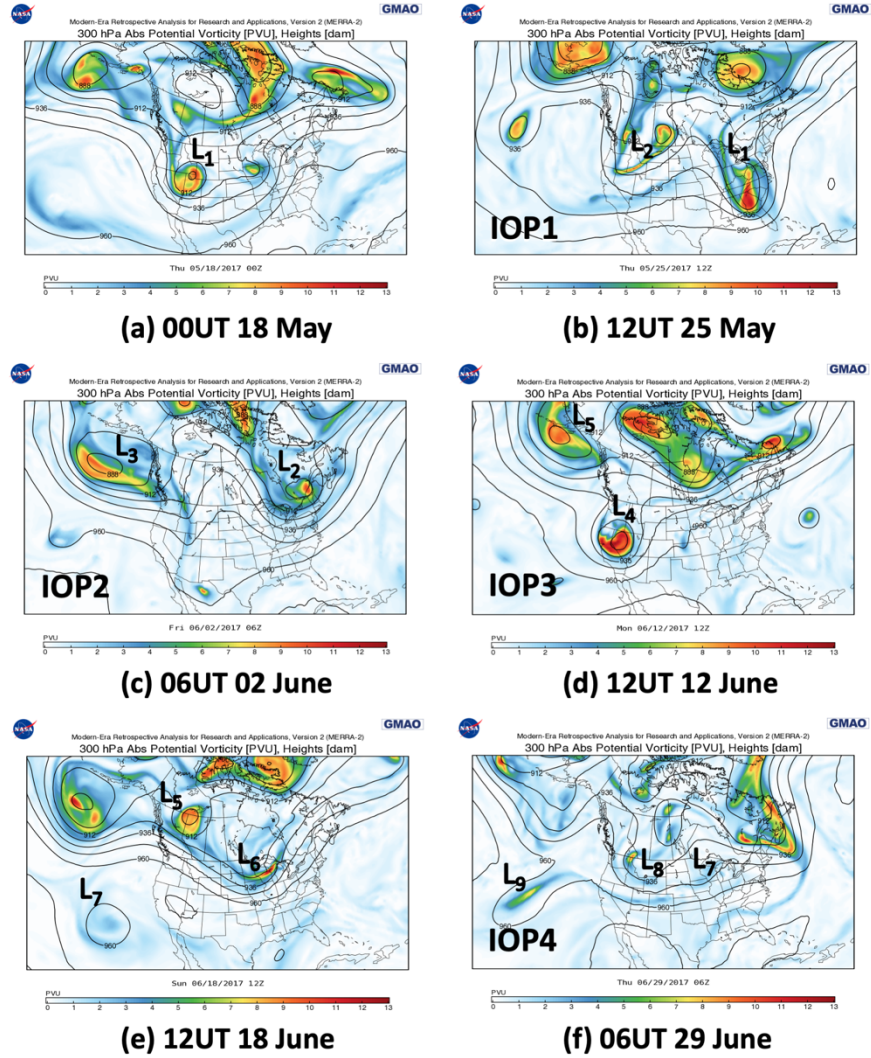


Figure 3: MERRA-2 300 hPa Absolute potential vorticity and geopotential heights (dam) at (a) 00UT 18 May, (b) 12UT 25 May, (c) 06UT 02 June, (d) 12UT 12 June, (e) 12UT 18 June, and (f) 06UT 29 June.

385

11-13 June. The O_3 and β profiles are summarized as time-height curtain plots in Figs. 4 and 5, respectively. The scalloped appearance of the individual curtains is caused by the diurnal variation in background solar radiation which determines the measurement signal-to-noise and thus the maximum achievable altitude. The dark gray curves show the boundary layer heights from the Doppler lidar and the red boxes outline the four IOPs. The colored stripe along the bottom of Fig. 4 shows the NLVA measurements from the *in-situ* monitor in the truck. Preliminary TOPAZ measurements from the afternoon of 17 May caught the remnants of a deep cyclonic intrusion from the closed low (L₁) in Fig. 3a, and free tropospheric layers and

390

filaments were present in nearly all of the profiles measured between mid-May to mid-June. The low backscatter in Fig. 5 shows that these layers were not created by biomass burning and most of the layers were higher (>4 km a.g.l) and more persistent than would be expected for pollution lofted from the Los Angeles Basin by the ‘mountain chimney effect’ 395 (Langford et al., 2010), but this process may have contributed to some of the lower-lying “residual layers” in the ozone curtains (e.g., 16 June). This suggests that most of the higher O_3 layers were stratospheric intrusions or Asian pollution plumes, a conclusion supported by the AM4 and GEOS-Chem simulations (Zhang et al., 2020). Free tropospheric O_3 layers appeared less frequently after the jet stream retreated into Canada, and photochemical production increased rapidly as the 400 subtropical ridge moved into the SWUS. The highest O_3 concentrations were usually measured in the boundary layer after mid-June, although Fig. 4 shows that this pattern was briefly interrupted on 18-19 June when the anticyclonic circulation transported clean marine air deep into the IMW. High O_3 was present both in and above the boundary layer during the last three days of the campaign when IOP4 was conducted.

The backscatter curtains in Fig. 5 show that TOPAZ measured relatively low backscatter during most of the campaign. The 405 aerosol loading was usually highest in the boundary layer, but comparisons to the near-IR Doppler lidar measurements and ozonesondes show that the gradients in the UV profiles were usually too weak to reliably define the boundary layer height. The backscatter above the top of the boundary layer increased abruptly on 19 June when smoke from fires in Arizona and Mexico drifted into the LVV, and high backscatter was measured both in and above the boundary layer on 20 June when smoke from the much closer Holcomb Fire reached Las Vegas. Note that the boundary layer height determination relied 410 heavily on the vertical velocity variance profile when dispersed smoke was present. These measurements will be described in more detail elsewhere along with those from 23-26 June when smoke from other regional wildfires reached Las Vegas and possibly contributed to the high surface O_3 measured on those days.

415

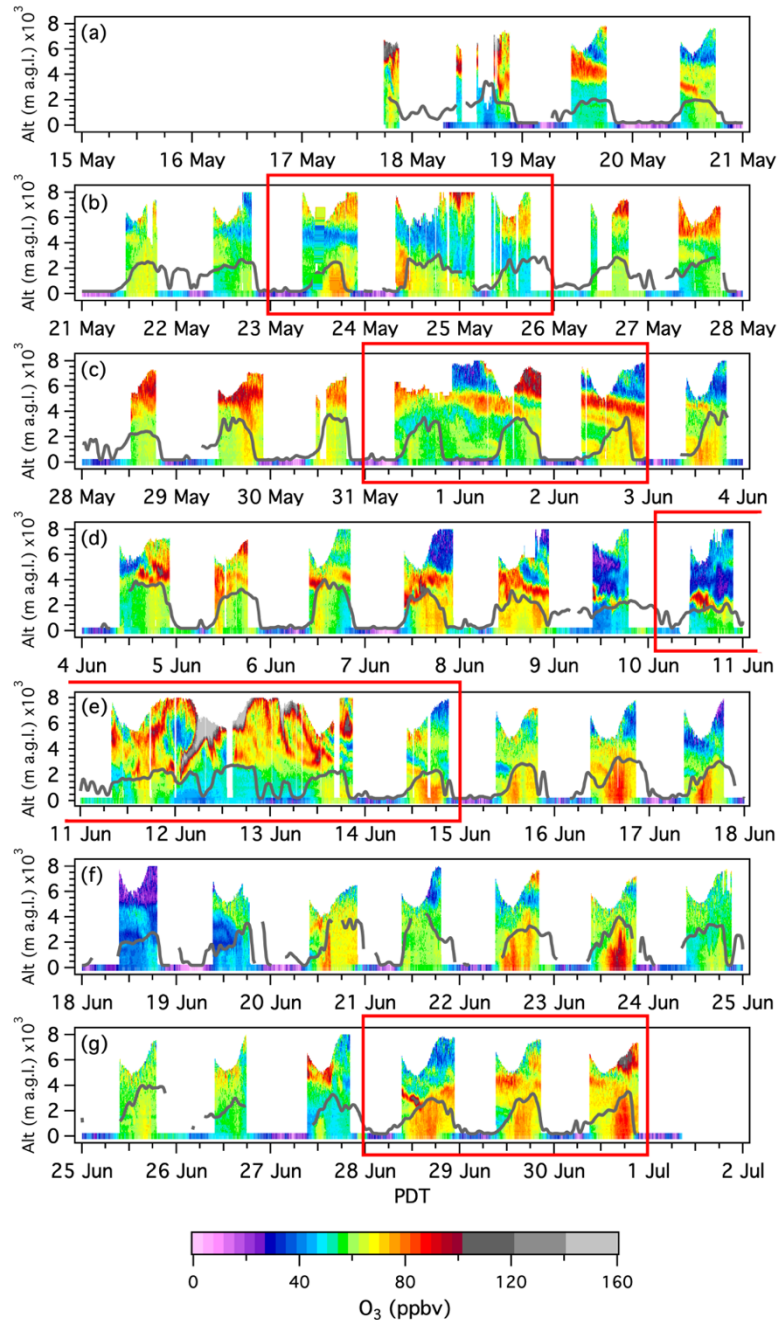


Figure 4: Time-height curtain plots showing the TOPAZ ozone measurements from the NLVA. The axes are altitude (Alt) above ground level and Pacific Daylight Time (PDT). The continuous ribbon along the bottom shows the measurements from the *in-situ* surface monitor in the TOPAZ truck and the dark gray curves show the boundary layer heights inferred from the co-located Doppler lidar measurements. The red boxes bracket the four IOPs.

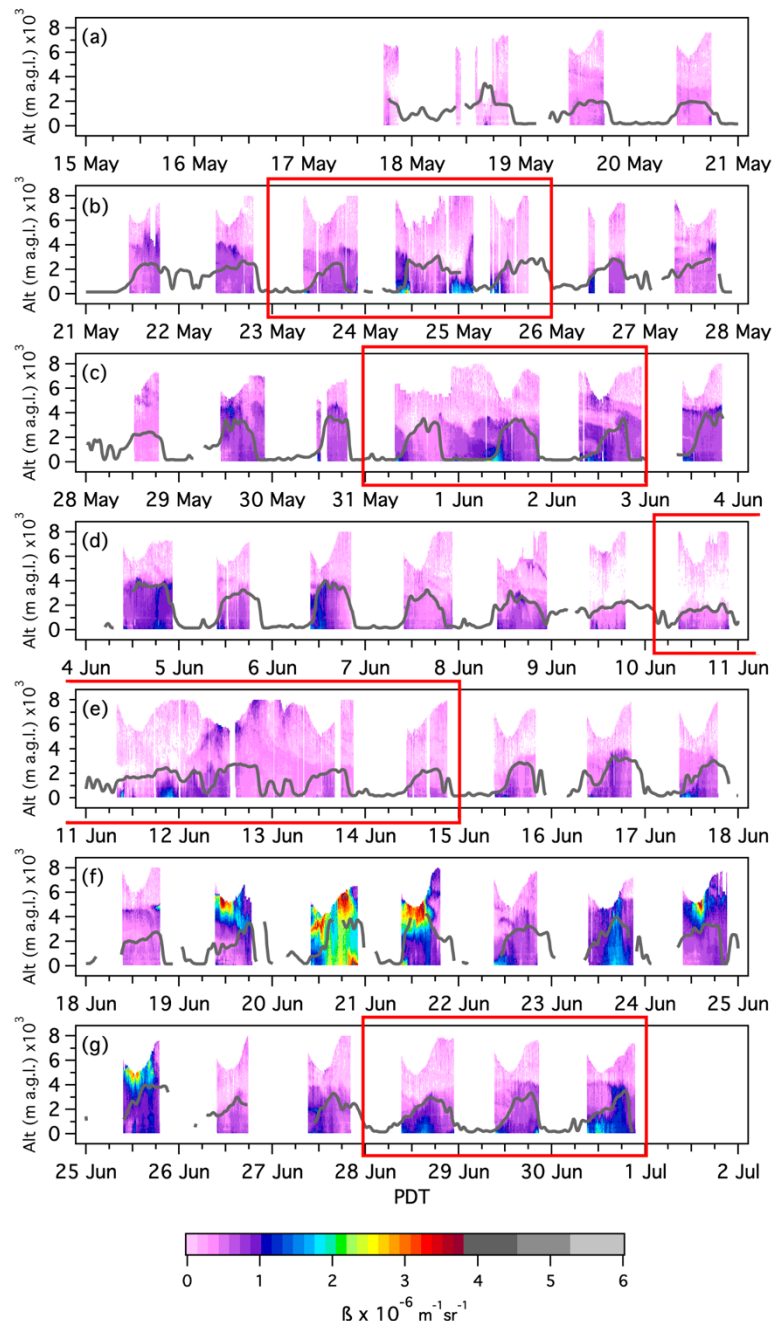
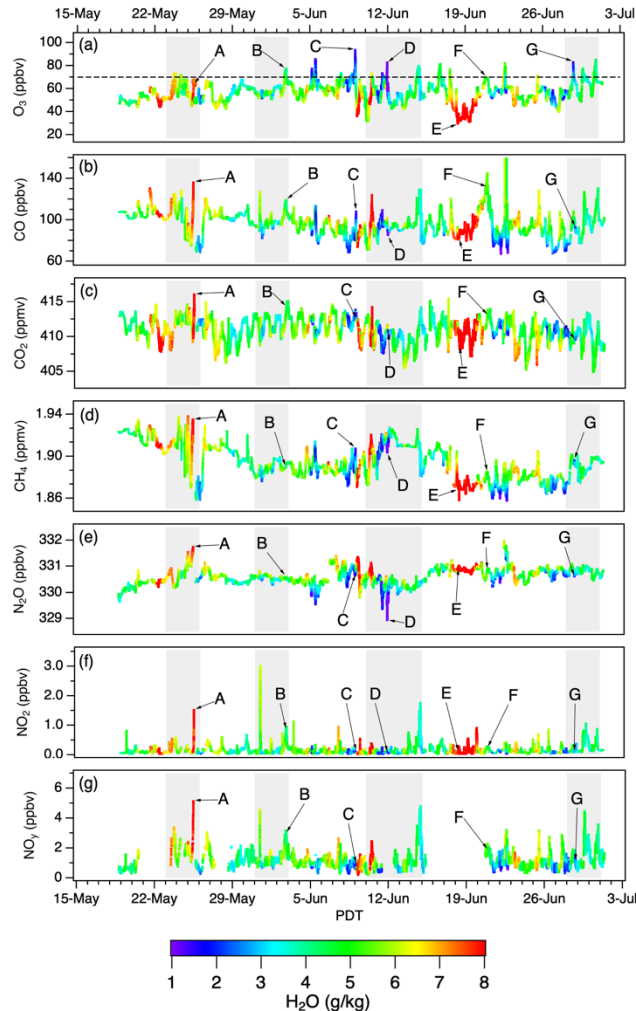


Figure 5: Same as Figure 4, but for the TOPAZ backscatter measurements.

425 **5.2 Mobile laboratory measurements**

The nearly continuous 1-min averaged *in-situ* O₃ measurements from the AP mobile laboratory are summarized in the top panel of Fig. 6; the lower panels plot the corresponding CO, CO₂, CH₄, N₂O, NO, NO₂, and NO_y measurements. As



430 **Figure 6: Time series of the AP 1-min *in-situ* measurements color-coded by the co-measured H₂O. The dashed black line in (a) shows the 2015 NAAQS of 70 ppbv. The gray regions bracket the four IOPs. The measurements labelled A-G are discussed in the text.**

noted above, the lack of rainfall and extreme aridity of the Mojave Desert allows us to use water vapor as a semi-conserved tracer and each of the time series is colorized by the co-measured H₂O to show whether the sampled air came from the lower

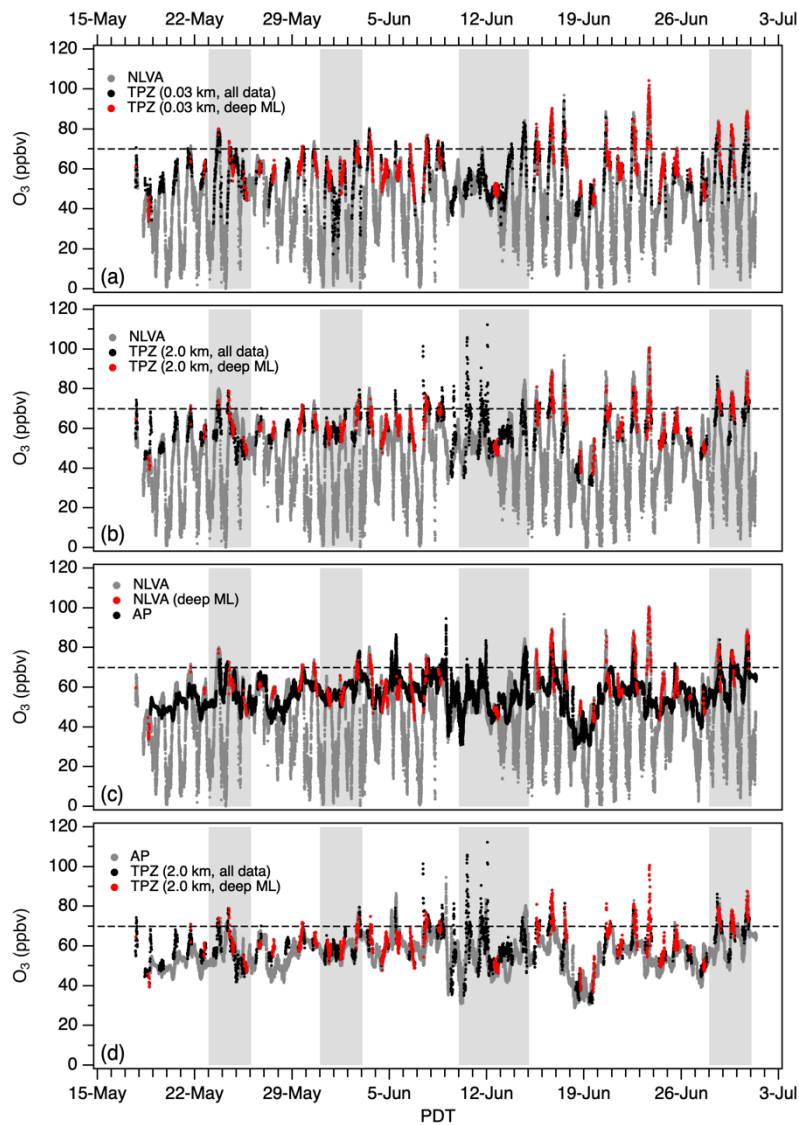
435 stratosphere or upper troposphere (dry: violet-blue) or from the terrestrial (moderate: green-yellow) or marine (moist: yellow-red) lower troposphere. The letters A-G identify specific transport episodes that will be examined in more detail below. The mobile laboratory measured 1-min O₃ mixing ratios in excess of 80 ppbv on 8 of the 43 measurement days in the campaign, and mixing ratios in excess of 70 ppbv on 17 days. The MDA8 O₃ averaged 60 ± 8 ppbv and exceeded the NAAQS on four days. Some of the highest O₃ concentrations were measured in very dry air with low NO₂ and NO_y during the night
440 and early morning (e.g., 8-9 June (episode C) and 11-12 June (episode D)), but high O₃ was also measured in more humid air with elevated NO₂ and NO_y on some afternoons (e.g., 2 June (episode B)). The AP wind measurements show that all of the short-lived nocturnal peaks coincided with strong south-westerly winds, while the broader afternoon peaks were associated with weaker south-easterly upslope flow. The lowest O₃ concentrations of the campaign were measured on 18-19 June in very moist air transported inland by the anticyclonic flow around the subtropical ridge seen centered over southern Nevada
445 in Fig. 3e.

5.3 Comparisons and validation

The vertical scanning capability of the TOPAZ lidar allows direct comparisons with nearby surface *in-situ* monitors. Fig. 7a compares time series of the O₃ mixing ratios retrieved at 27.5 ± 5 m a.g.l. (red) with the *in-situ* measurements sampled 5 m
450 a.g.l. at the truck (gray). The two series are in excellent agreement ($\pm 1\%$, $R^2=0.91$) when the co-located Doppler lidar showed that the boundary layer to be >2500 m deep (black). The TOPAZ lidar was not normally run overnight, but Fig. 7a shows that the only significant differences between the time series occurred during a 24-hour run through the night of 31 May – 1 June (IOP2) when O₃ near the truck was titrated by NO emitted from nearby combustion sources. These emissions did not affect the TOPAZ concentrations retrieved about 20 m high and 800 m down range. The nocturnal losses were much
455 smaller on 25 May and 7-12 June when winds from the passing cold fronts dispersed the NO_x emissions and disrupted the shallow nocturnal inversion layers. Fig. 7b is similar to Fig. 7a, but compares the NLVA *in-situ* measurements with the TOPAZ mixing ratios at 2000 m a.g.l., the elevation of AP. Although TOPAZ frequently measured higher O₃ aloft on 7-12 June when the boundary layer was relatively shallow (Fig. S1), these measurements are also in good agreement ($\pm 1\%$, $R^2=0.76$) when the boundary layer was deeper than 2500 m.

460 Fig. 7c compares the *in-situ* measurements from the NLVA (gray) with those from AP (red). The most obvious difference between the time series is the lack of surface deposition and NO_x titration on AP, which was exposed to free tropospheric air during the night. The black points show that mixing ratios were similar ($\pm 4\%$, $R^2=0.46$) when the boundary layer above the NLVA was >2500 m. One notable exception are the measurements from 23 June when the measurements in the LVV may
465 have been influenced by smoke from the Brian Head Fire in southwestern Utah (cf. Fig. 5f). Although difficult to see in Fig. 7c, the AP O₃ concentrations typically lagged those at the NLVA on days with well-developed upslope flow, including the four AP exceedance days (14, 16, 29, and 30 June). A key assumption of the *FAST-LVOS* experimental design was that the air sampled on the summit of AP was representative of the air entrained by the mixed layer above the LVV. The similarity

between the 2000 m a.g.l. TOPAZ retrievals and the mobile laboratory O₃ measurements in Fig. 7d show that this was generally the case when the boundary layer was >2500 m deep. The time series are in good agreement ($\pm 4\%$, $R^2 = 0.60$) under these conditions if the measurements from 23 June are excluded.



475 **Figure 7:** Time series comparing the TOPAZ O₃ mixing ratios with the NLVA and AP *in-situ* measurements. (a) TPZ (0.03 km) and NLVA surface monitor in the TOPAZ truck, (b) TPZ 2.0 km a.g.l. and NLVA surface monitor, and (c) NLVA and AP surface monitors, and (d) TPZ 2.0 km a.g.l. and AP surface monitor. The gray bands show the four IOPs. The horizontal dashed lines show the 2015 NAAQS of 70 ppbv. The red points highlight measurements made when the mixed layer was more than 2500 m deep.

480 6 Intensive operating periods

The aircraft and ozonesonde profiles acquired during the four IOPs provided spatial context for the lidar measurements and helped distinguish stratospheric intrusions from Asian pollution. The planning and successful execution of these intensives relied on the ability of the RAQMS (96 h) and RAP-Chem (48 h) models to predict stratospheric intrusion and pollution transport events more than 48 hours in advance so that the aircraft and ozonesonde teams could return to Las Vegas from 485 their home stations. Examples of the model forecasts are shown in Fig. 8, which displays the O₃ and CO forecasts for 12UT 12 June

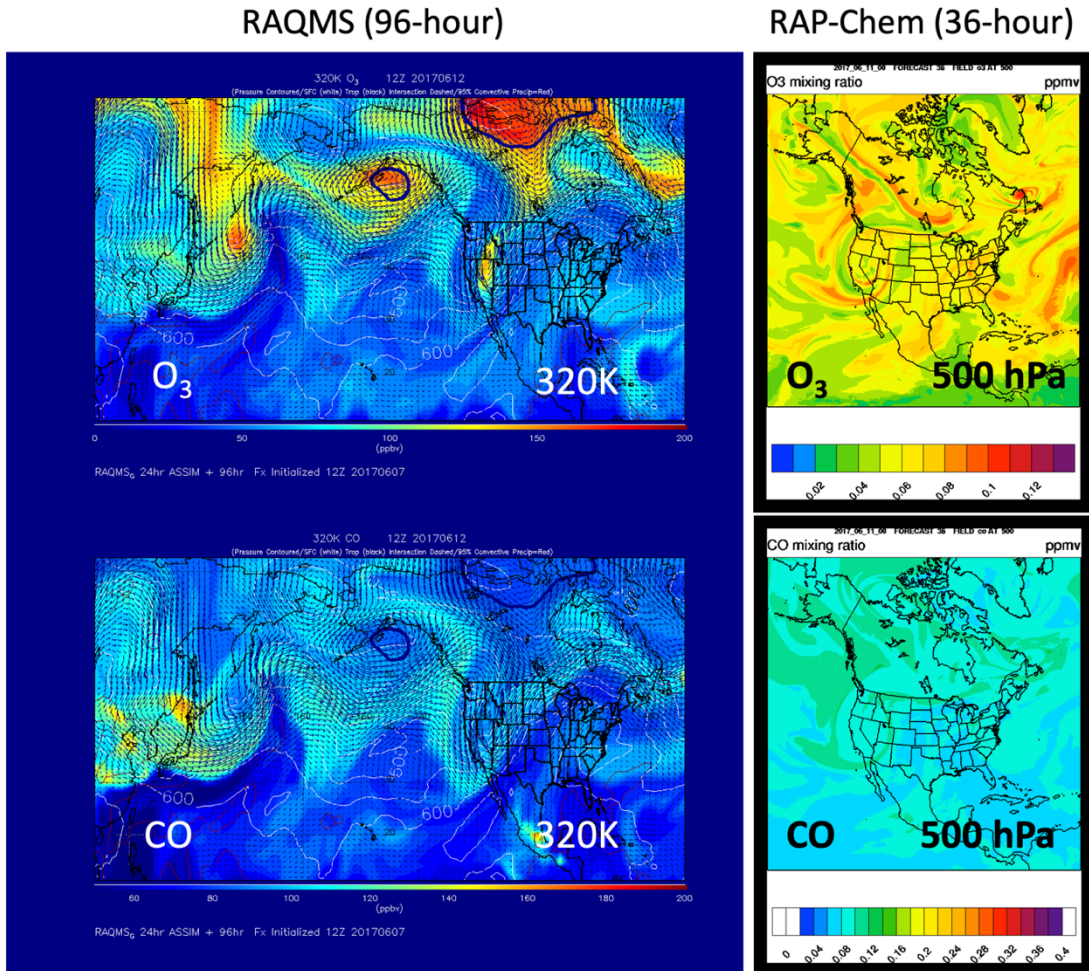


Figure 8: RAQMS (left) and RAP-Chem (right) O₃ (top) and CO (bottom) forecasts for 12UT 12 June 2017. The 320 K RAQMS forecasts were initialized at 12UT 7 June; the 500 hPa RAP-Chem forecasts at 00UT 11 June.

490 (cf. Fig. 3d). The left panels of Fig. 8 show the 96-hour total O₃ (top) and CO (bottom) at 320K (\approx 500 hPa or 5.8 km a.s.l. above Las Vegas) from RAQMS initialized at 12UT on 7 June, and the right panels show the 36-hour RAP-Chem O₃ and

CO 500 hPa forecasts initialized at 00UT on 11 June. Note that the higher resolution RAP-Chem model gets its boundary conditions from the RAQMS model. This example shows that the RAQMS model captured both the timing and location of the stratospheric intrusion/Asian pollution event 4 days out or 3 days before the start of IOP3 on 10 June. The retrospective 495 MERRA-2 PV analyses in Fig. 3, and FLEXPART stratospheric ozone (STTO3) and Asian CO (ASIACO) tracer distributions (<https://csl.noaa.gov/projects/fastlvos/FAST-LVOSfinalreport604318-16.pdf>, last access 7 December 2021) in Figs. 9 and 10, respectively, show that stratospheric air and/or Asian pollution was present in the middle and upper troposphere above Nevada during each of the IOPs. The correspondence between the 96-h RAQMS forecasts in Fig. 8 and the retrospective FLEXPART distributions in the third columns of Figs. 9 and 10 is particularly impressive.

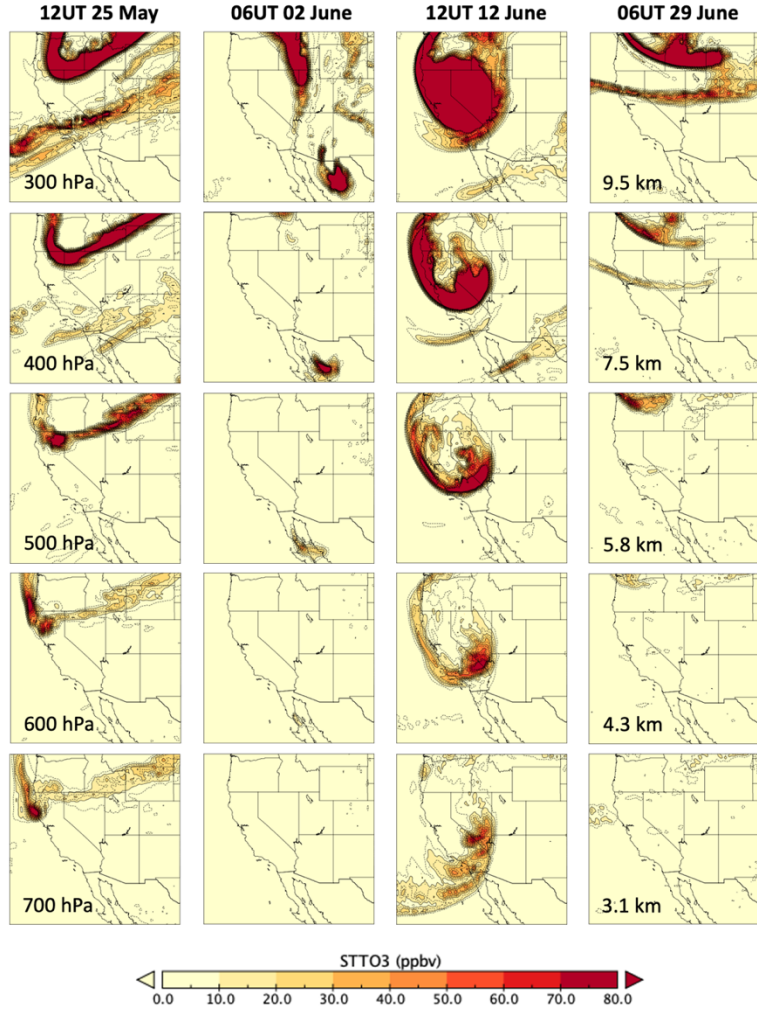
500

The curtain plots in Fig. 4 show that the TOPAZ lidar measured high O₃ in the middle and upper troposphere during each of the IOPs; the expanded 3-day curtain plots in Figs. 11-14 show these measurements in more detail. The superimposed horizontal ribbons represent the NLVA and AP surface measurements and the nearly vertical ribbons the ascending profiles from the ozonesondes. Those portions of the descending profiles within 20 km of the NLVA are also plotted. The NLVA and 505 AP surface wind measurements and continuous Doppler lidar boundary layer heights are also overlaid on the curtains, with the boundary layer heights derived from the ozonesonde potential temperature profiles (black open circles) plotted for comparison. The heavy arrows at the top of each plot corresponds to the MERRA-2 analyses in Fig. 3. The labels A, B, D, and G match the corresponding peaks in Fig. 6.

510 The SA aircraft profiles overlap with the midday ozonesonde profiles and are omitted from the curtain plots for clarity, but Fig. 15 shows longitudinal transects of the sections of the outbound (left) and inbound (right) flight legs between the NLVA and AP on 25 May (IOP1), 2 June (IOP2), 12 June (IOP3), and 28 June (IOP4). The flight tracks are colorized by the O₃ measurements, and the plots also show the mean lidar and ozonesonde profiles and surface O₃ measurements from the roughly 1-hour interval bracketing the NLVA and AP profiles. Ozonesondes were only launched between 0900 and 1500 515 PDT and thus did not overlap with the return flight legs. These plots underscore the good agreement between the different *FAST-LVOS* O₃ measurements, and support the assumption that the air above AP was usually representative of the air above the LVV. Similar plots colorized by H₂O and CH₄ are displayed in Figs. S2 and S3. Fig. 16 shows the measured O₃ mixing ratios along the outbound flight legs from the NLVA to Big Bear, and the inbound flight legs back to Jean. The AP profiles and TOPAZ measurements are omitted from these plots as are the afternoon profiles above the LVV. In the following 520 sections, we briefly describe each of the IOPs and compare the upper air measurements with the FLEXPART STTO3 and ASIACO tracer distributions. More complete descriptions of these measurements are planned for future publications.

6.1 IOP1: 23 May-25 May

525 The first IOP was timed to coincide with the arrival of the trough (L_2) poised above the northern IMW in Fig. 3b. The PV analysis for the morning (12UT) of 25 May shows a deep cyclonic intrusion wrapping around L_2 , and the FLEXPART STTO3 plots in the first column of Fig. 9 show a deep cyclonic intrusion descending almost vertically to 700 hPa above northern Nevada and California. The PV analysis in Fig. 3b also shows a thin anticyclonic streamer stretching across southern Nevada

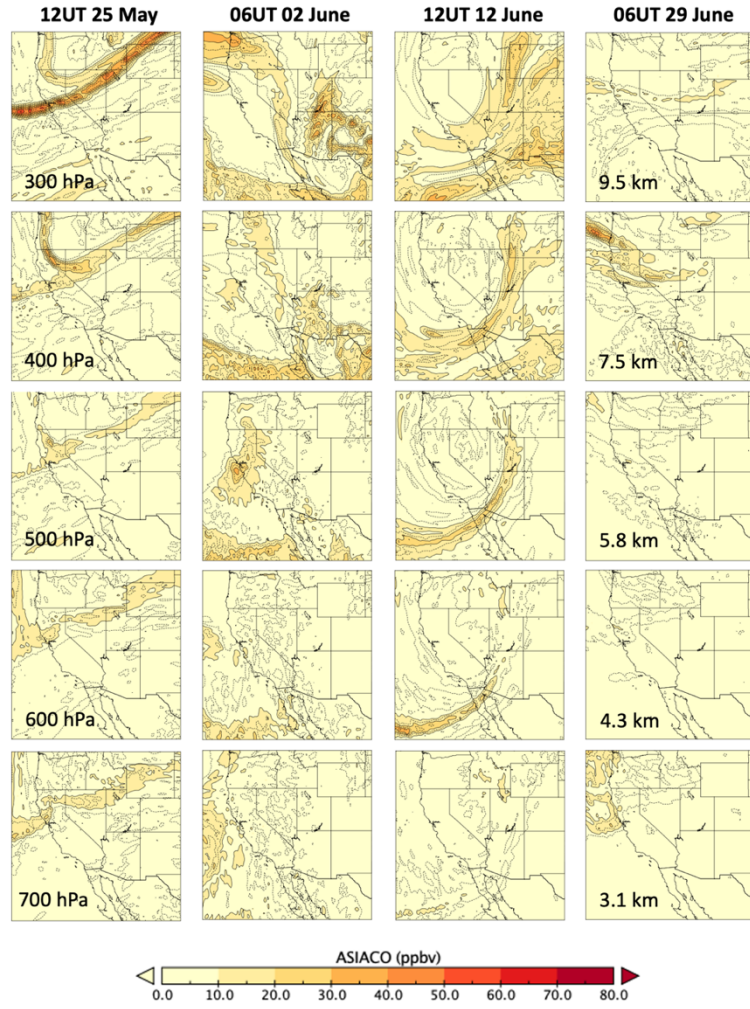


530

Figure 9: FLEXPART STTO3 tracer distributions during the four IOPs. The plots show the distributions, from left to right, at 12UT 25 May, 00UT 02 June, 12UT 12 June, and 06UT 29 June, and from top to bottom, 300, 400, 500, 600, and 700 hPa. The approximate altitudes a.s.l. near Las Vegas corresponding to the different pressure surfaces are shown in the panels on the far right. The heavy black contour lines (e.g., in the upper left panel) indicate that the scale is saturated.

535 from the tip of L_1 , now an elongated trough over the eastern U.S., and FLEXPART shows this shallower feature on the 300 and 400 hPa surfaces. The ASIACO tracer distributions in the first column of Fig. 10 show Asian pollution mingled with the

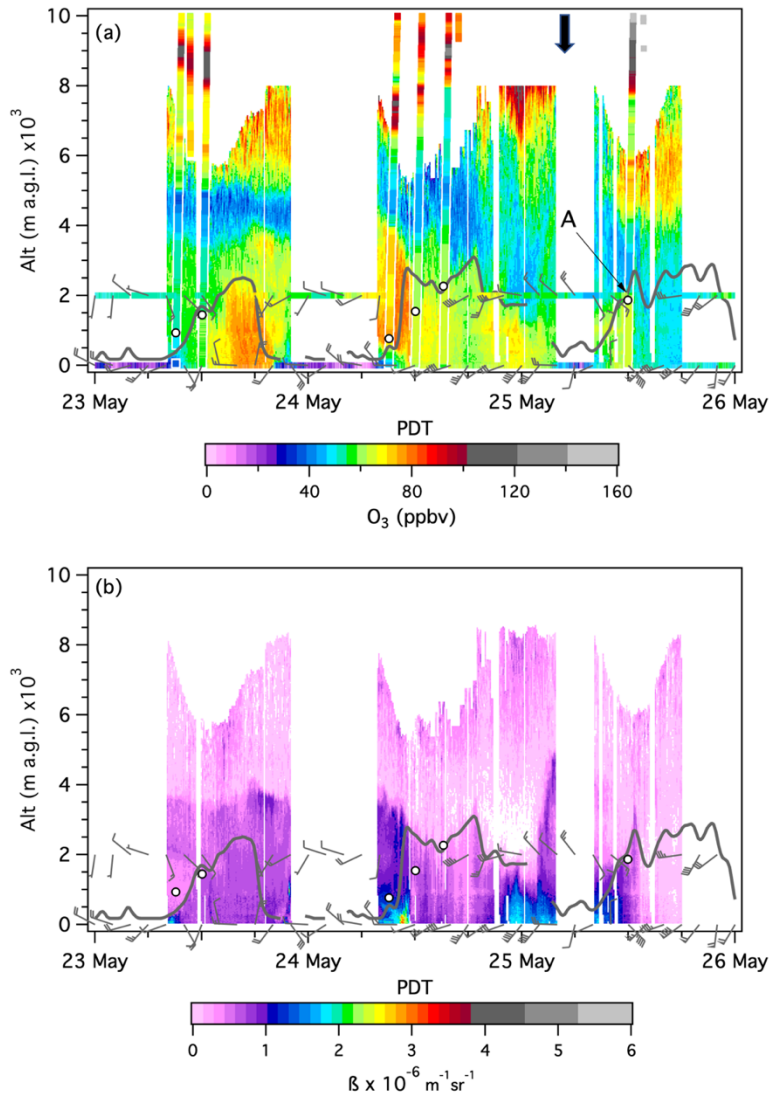
cyclonic intrusion, and in a deep narrow band stretching across northern Nevada between the cyclonic and anticyclonic intrusions. Analysis of satellite CO measurements and the GFDL-AM4 and GEOS-Chem model simulations by *Zhang et al.* (2020) also found a large Asian pollution component in these layers.



540

Figure 10: Same as Fig. 9, but for the ASIACO tracer.

The curtain plots for 23-25 May in Fig. 11 show layers with more than 100 ppbv of O₃ above the LVV on all three days, but 545 the layers were above the \approx 6 km a.s.l. altitude ceiling of the SA Mooney on the first two days. The aircraft was able to reach the more diffuse band with 75 to 80 ppbv of O₃ seen above 4.5 km a.g.l. on 25 May, however, and the plots in Figs. 15 and 16 show that this layer extended to the south at least as far as Barstow (cf. Fig. 1).



555 **Figure 11:** Time-height curtain plots similar to those in Figures 4 and 5, but expanded to better show the TOPAZ (a) ozone and (b) backscatter measurements during IOP1. The dark gray curves represent the boundary layer heights derived from the co-located Doppler lidar measurements. The superimposed horizontal bands in (a) show the AP and NLVA *in-situ* O_3 measurements and the near-vertical colored bands show the Joe Neal ozonesonde profiles. The barbs in both panels show the AP and NLVA surface winds and the open circles the mixing heights inferred from the ozonesondes. The heavy black arrow above (a) corresponds to the 12UT 25 May PV plot from Figure 3b. The 300 hPa surface lies at approximately 9 km a.g.l. The label “A” is the same as in Figure 6.

560 Figs. S3 shows that the air in this layer was extremely dry, but the absence of a corresponding CH₄ enhancement in Fig. S4 suggests that this layer was primarily of stratospheric origin. The lidar, aircraft, and ozonesonde measurements also show that the high O₃ aloft was separated from the boundary layer by a layer of continental air with much lower O₃ concentrations, and there was no obvious local mixing of the O₃ aloft into the boundary layer. The GFDL-AM4 simulations also found little evidence for stratospheric or Asian pollution influences in Clark County surface air, but estimated Asian contributions of 8-
565 15 ppbv of O₃ to the surface along the areas of northern California, Idaho, and Wyoming lying beneath the bands seen in the 700 hPa STTO3 and ASIACO FLEXPART analyses.

The GFDL-AM4 and GEOS-Chem models did show large contributions from local and regional pollution in the lowest few kilometres above Clark County during IOP1, and the TOPAZ curtain plots also show moderately high (70-80 ppbv) O₃ in the 570 boundary layer on 23 May, and what appears to be a residual layer with 70-80 ppbv of O₃ and high β above the boundary layer on the morning of 24 May. The lidar also found 60-70 ppbv of O₃ with high β in the boundary layer on the morning of 25 May that decreased abruptly when the winds rotated to the southwest just after noon. These measurements correspond to episode A in Fig. 6, and the outbound aircraft measurements plotted in the top panels of Figs. S2 and S3 show that the air above the LVV and AP was relatively moist and enriched in CH₄. The mobile laboratory also found moist air with moderate 575 O₃ on AP, but also measured elevated CO, CH₄, CO₂, N₂O, and the highest NO_y concentrations measured during the campaign. The scatter plots in Fig. 17 show that O₃ was positively correlated with all of these tracers and a 96-h HYSPLIT back trajectory launched 2 km above the NLVA (Fig. 18, solid red line) meandered around the southern San Joaquin Valley (SJV) within the shallow boundary layer in the valley which is typically less than 1 km deep in summer (Faloona et al., 2020) for more than 48 hours before exiting through the Tejon Pass and crossing the Mojave Desert to Las Vegas. This can 580 explain the high N₂O and CH₄ concentrations, which likely came from agricultural and oil and gas sources in the SJV. The air parcel was also exposed to urban sources in the SJV and the high CO₂ and NO₂ concentrations show that the parcel entrained additional urban pollution as it passed through the LVV en route to AP.

585 This interesting case illustrates yet another way that passing troughs can influence surface air quality in the LVV. Fig. 18 shows that the trajectory initially followed the cyclonic circulation from L₂ (cf. Fig. 3b) southward along the California coast (hence the high moisture content) before crossing the Coastal Mountains into the SJV on 23 May. The parcel then followed the circulation northward into the LVV as the trough moved east. The influence of the synoptic flow on the low-level winds is also seen in the transport to AP, which occurred in the early morning and several hours before the thermally forced upslope flow became established.

590

6.2 IOP2: 31 May-2 June

The second IOP focused on one in a series of shallow upper-level lows that spun off of the Aleutian Low in late May and early June. The MERRA-2 analysis for 06UT 2 June in Fig. 3c shows the low (L_3) approaching the Pacific Northwest. A narrow filament of high PV air emanating from the low stretches anticyclonically above the Nevada-Utah border, but the

595

corresponding FLEXPART STTO3 distributions in the second column of Fig. 9 suggest that the intrusion was quite shallow. The ASIACO distributions in Fig. 10 show bands of Asian pollution on both sides of the stratospheric filament, with the pollution descending to at least 400 hPa above California. The TOPAZ and ozonesonde measurements in Fig. 12a show two

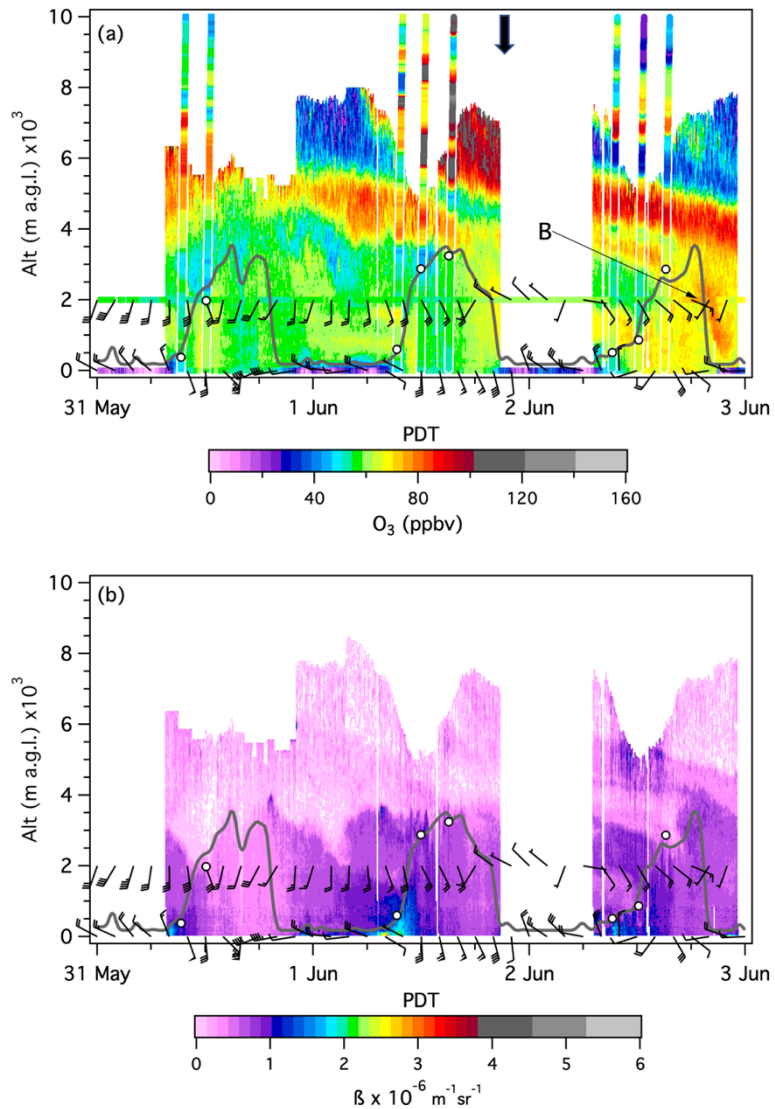


Figure 12: Same as Figure 11, but for IOP2. The heavy black arrow corresponds to the 06UT 2 June 300 hPa plot in Figure 3c.

600 downward sloping bands of high O₃ between the top of the convective mixed layer and \approx 9 km a.g.l. on the afternoon of 1 June, with the lowermost band appearing to merge with the mixed layer on the afternoon of 2 June. The backscatter curtains in Fig. 12b also show slightly higher β in the uppermost layer at 5 km a.g.l., than in the lower one at 4 km a.g.l.

605 The aircraft and ozonesonde profiles in Fig. 15 also show the two O₃ layers above the LVV in the morning, but the aircraft measurements show little indication of the lower layer in the profile above AP, and Fig. 16 shows it to have been rather tenuous between Las Vegas and Barstow. Figs. S2 and S3 show that both layers were very dry (3-8% RH), but only the uppermost layer was elevated in CH₄. This, together with the backscatter measurements in Fig. 12b suggests that the upper layer was mostly Asian pollution while the lower layer was mostly stratospheric. The TOPAZ curtain plot and afternoon aircraft profiles show that the convective boundary layer completely entrained the lower (stratospheric) layer and reached the 610 bottom of the upper (Asian pollution) layer where some entrainment must also have taken place.

615 The mobile laboratory measurements from AP in Figs. 6 and 17 show a pronounced O₃ peak on the afternoon of 2 June (episode B), but the other tracers show that this peak was caused by continental air and not the stratospheric intrusion or Asian pollution plume, consistent with the model-based attribution of the 2 June O₃ peak to regional pollution (Zhang et al., 2020). The sampled air had typical tropospheric N₂O concentrations and elevated CO, CO₂, NO₂ and NO_y concentrations consistent with anthropogenic pollution. The high NO₂/NO_y ratio points to local sources and the wind barbs in Fig. 12 show that the air was transported up Kyle Canyon from the LVV by the afternoon upslope flow. The HYSPLIT trajectory in Fig. 18 (green line) approaches southern Nevada from the southeast without passing over California or any of the fires burning in Mexico and Arizona at the time. Similar local upslope events occurred frequently in late June (14, 16, 22, and 30 June) after 620 the subtropical ridge became established.

6.3 IOP3: 10 June-14 June

625 The third IOP was triggered by another deep closed low (L₄) that moved into the western U.S. in the second week of June. This cyclonic system was unusually deep for mid-June and the PV plot for 12UT on 12 June in Fig. 3d appears very similar to that for 00UT 18 May (Fig. 3a). The cold front brought strong (>10 m s⁻¹) south-south-westerly winds to Clark County and freezing temperatures (-5°C) to AP on the night of 11-12 June (Fig. S1). The FLEXPART STTO3 analyses in Fig. 9 show a deep cyclonic stratospheric intrusion descending to at least 700 hPa over southern Nevada, and the corresponding ASIACO analyses in Fig. 10 show cyclonic bands of pollution descending ahead of the stratospheric air. The RAQMS and RAP-Chem forecast plots in Fig. 8 appear similar.

630

The third IOP was extended to 5 days (10-14 June) with aircraft sorties flown on all 5 days and ozonesondes launched on 4 (10-13 June). The curtain plot in Fig. 13a shows a continuous TOPAZ run of 60 hours lasting from 0800 PDT on 11 June to 2100 PDT on 13 June. The lidar and superimposed ozonesonde profiles show a complex network of O₃ filaments descending

into the lower troposphere with more than 150 ppbv of O₃ approaching to within 3.3 km of the surface at ≈0300 PDT on 12

635 June, and ≈250 ppbv measured at 5.5. km a.g.l. around 0900 PDT. The aircraft, ozonesonde, and lidar profiles in Fig. 15

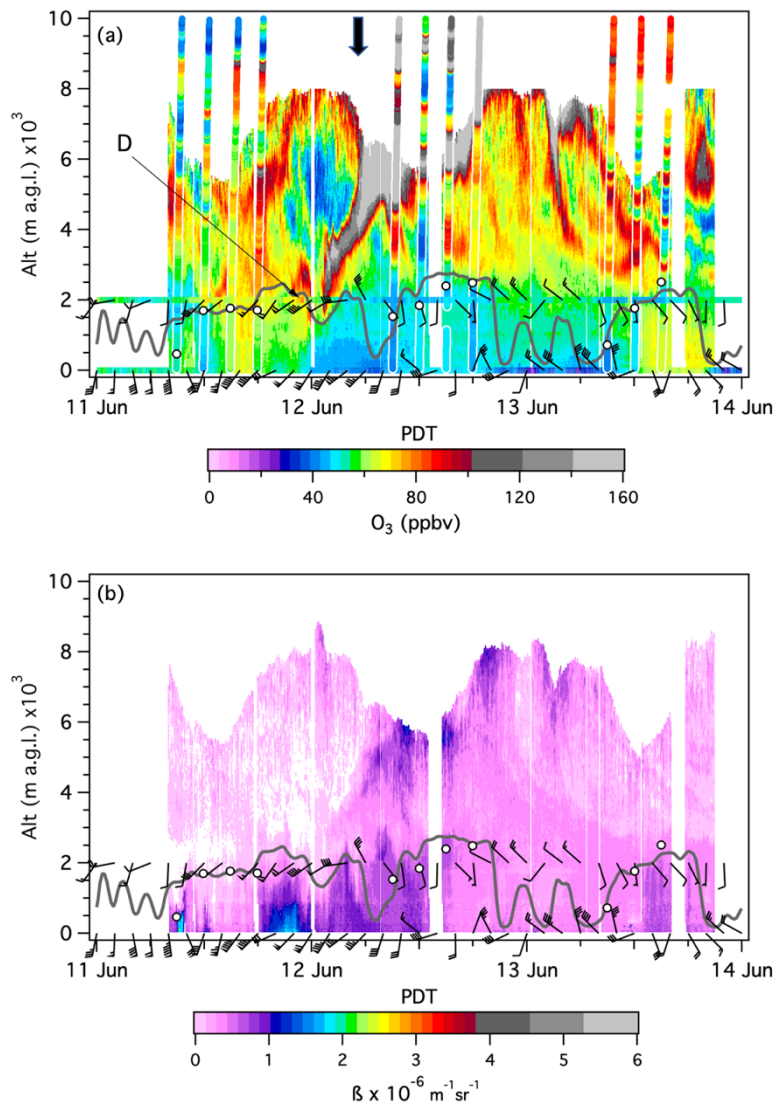


Figure 13: Same as Figure 11, but for IOP3. The heavy black arrow corresponds to the 12UT 12 June 300 hPa plot in Figure 3d.

640

show more than 120 ppbv of O₃ between 6 and 8 km a.g.l. in the early afternoon of 12 June, and Fig. 16 shows the intrusion sloping downward to the south with more than 140 ppbv measured along the 5.5 km a.s.l. flight leg between Barstow and Jean. The profiles near the NLVA and AP also show elevated CH₄ in the air above and below the high O₃ layer (Fig. S4),

which along with the elevated backscatter beneath the tongue in Fig. 13b shows the Asian pollution descending ahead of the

645 stratospheric air.

Fig. 13a shows that the O_3 maximum of 84 ppbv recorded around 2300 PDT on 11 June by the mobile laboratory on AP (episode D) occurred close to the deepest penetration of the intrusion in the lidar curtain. The sampled air was extremely dry

($\approx 0.1\%$ H_2O) and the stratospheric origin confirmed by the low N_2O concentrations in Fig. 6 and the negative correlations of

650 O_3 with CO, CH_4 , and N_2O in Fig. 17. The NO_y converter was offline during this episode, but the NO_x concentrations were near the detection limit. Similar chemical characteristics were measured in the air sampled during the first of the two O_3 peaks that appeared on the morning of 5 June and mentioned in **Section 5.2**. Fig. 18 (purple line) shows the HYSPLIT back trajectory descending from the northwest over the previous 72 hours.

655 Interestingly, this large intrusion did not lead to particularly high surface O_3 in the LVV on 11-13 June since the high winds from the cold front dispersed most of the locally produced O_3 and other pollutants ahead of the descending stratospheric air (Langford et al., 2012). The curtain plots do show a short-lived increase in the lowest 2 km on the afternoon of 11 June when the surface O_3 concentrations briefly climbed from 50 to 70 ppbv at the NLVA. However, the GFDL-AM4 model suggests that the intrusion layer was mixed into regional pollution on June 13-14 and pushed the MDA8 O_3 to exceed the 70 ppbv

660 NAAQS level at sites across the SWUS, including several sites in Clark County (Zhang et al., 2020). Once stratospheric air is mixed into local pollution, it loses its key stratospheric characteristics (e.g., low CO and low H_2O), challenging diagnosis of its surface impacts directly based on observations. This case study demonstrates the importance of integrating observational and modeling analysis for the unambiguous attribution of high- O_3 events in the SWUS (Zhang et al., 2020).

665 6.4 IOP4: 27 June-30 June

The final IOP targeted a weak trough (L_8) that crossed the Canadian border near the end of June. The MERRA-2 analysis for 06UT 29 June (Fig. 3f) shows the PV maximum on the western flank of the trough. The analysis also shows the latest (L_8) in a series of cut-off lows (COL) (Nieto et al., 2005) that formed off the coast of California in late June. These COLs typically

670 meandered around the Eastern Pacific for several days before re-joining the main flow, and Fig. 3f shows a narrow filament connecting L_9 to the remnants of L_7 (cf. Fig. 3e), which now lies above the Midwest. The FLEXPART STTO3 tracer in Fig. 9 shows both a cyclonic intrusion from L_8 descending to 500-600 hPa above Oregon, and the narrow filament connecting the two COLs above southern Nevada on the 400 hPa surface. Fig. 10 shows that there was significant Asian pollution between the filament and the cyclonic intrusion.

675 The TOPAZ curtain plot in Fig. 14 shows high (> 80 ppbv) O_3 above the boundary layer on 29 and 30 June, with up to 90 ppbv measured in the boundary layer on 30 June. The SA profiles from these days (not shown) found very dry air with depressed CH_4 concentrations in the O_3 -rich layers above 4 km a.g.l. suggesting that they originated in the stratosphere. The

most interesting measurements are those from 28 June, however, which show a thin layer with more than 100 ppbv of O₃, but low β disappearing into the convective mixed layer in the early afternoon, the most striking example of boundary layer entrainment observed during *FAST-LVOS*. The companion paper by *Zhang et al. (2020)* refers to this as an “unattributed event” since the layer was not resolved by either the AM4 (C192: $\approx 50 \times 50 \text{ km}^2$ horizontal, $\approx 200 \text{ m}$ vertical) or GEOS-Chem () global models, and cannot be resolved by FLEXPART for that matter. The spatial inhomogeneity of the layer is evidenced by the aircraft measurements in Figs. 15 and 16. Fig. S3 shows that the air was very dry both within and above the mystery layer, and the combination of extreme dryness and low β rules out biomass burning or regional pollution. The layer was also rich in CH₄ suggesting that it was not a stratospheric intrusion.

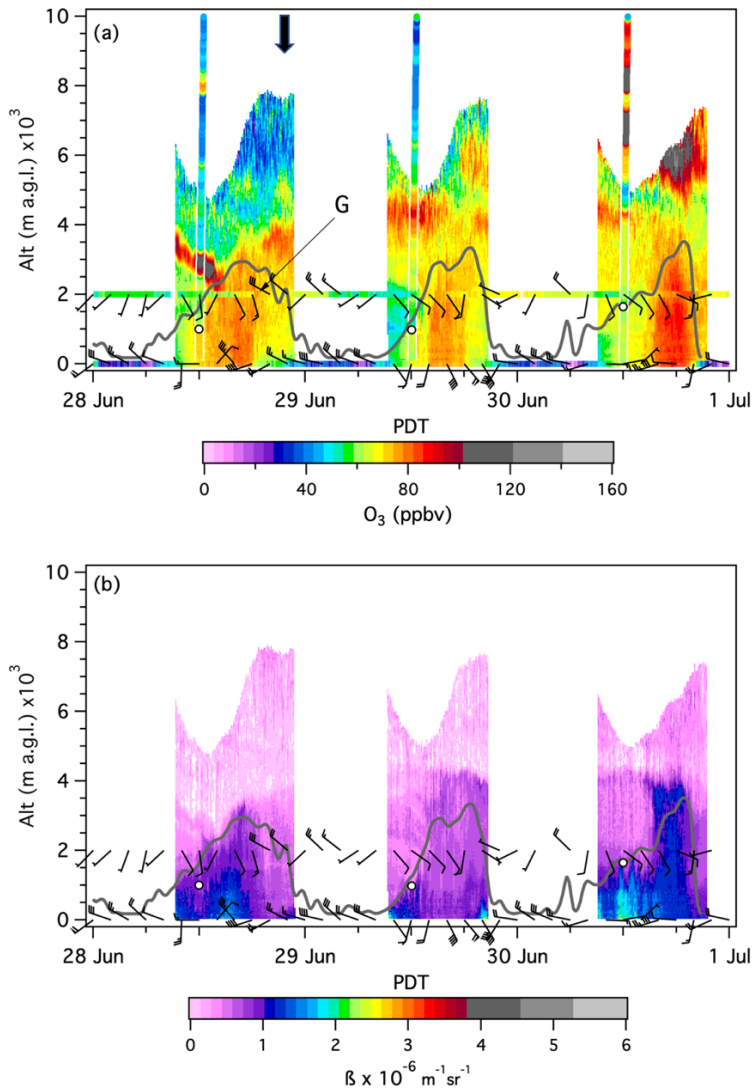
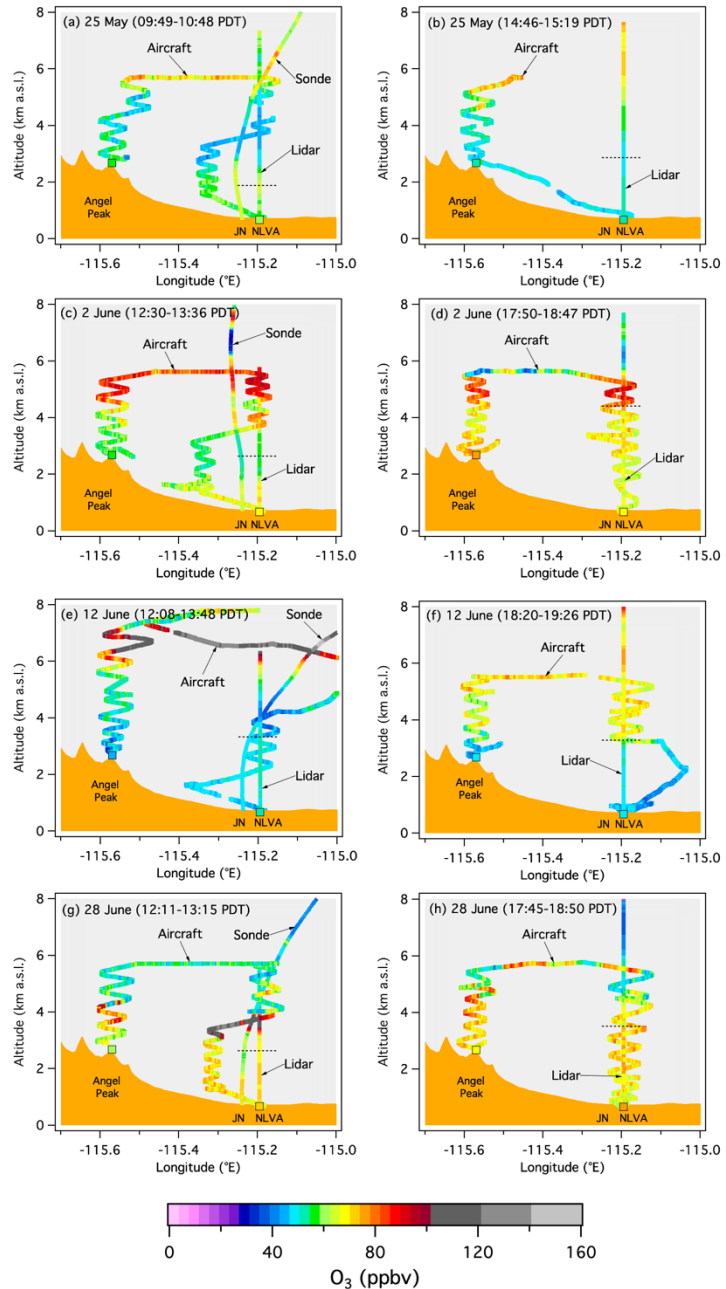


Figure 14: Same as Figure 11, but for IOP4. The heavy black arrow corresponds to the 00UT 29 June 300 hPa plot in Figure 3f.



690 **Figure 15:** Ozone mixing ratios measured by the lidar, ozonesonde, and aircraft, and by the AP, Joe Neal (JN), and NLVA surface monitors during the outgoing (left) and returning (right) flights on: (a), (b) 25 May, (c), (d) 2 June, (e), (f) 12 June, and (g), (h) 28 June. The horizontal dashed lines show the boundary layer height inferred from the NLVA Doppler lidar measurements.

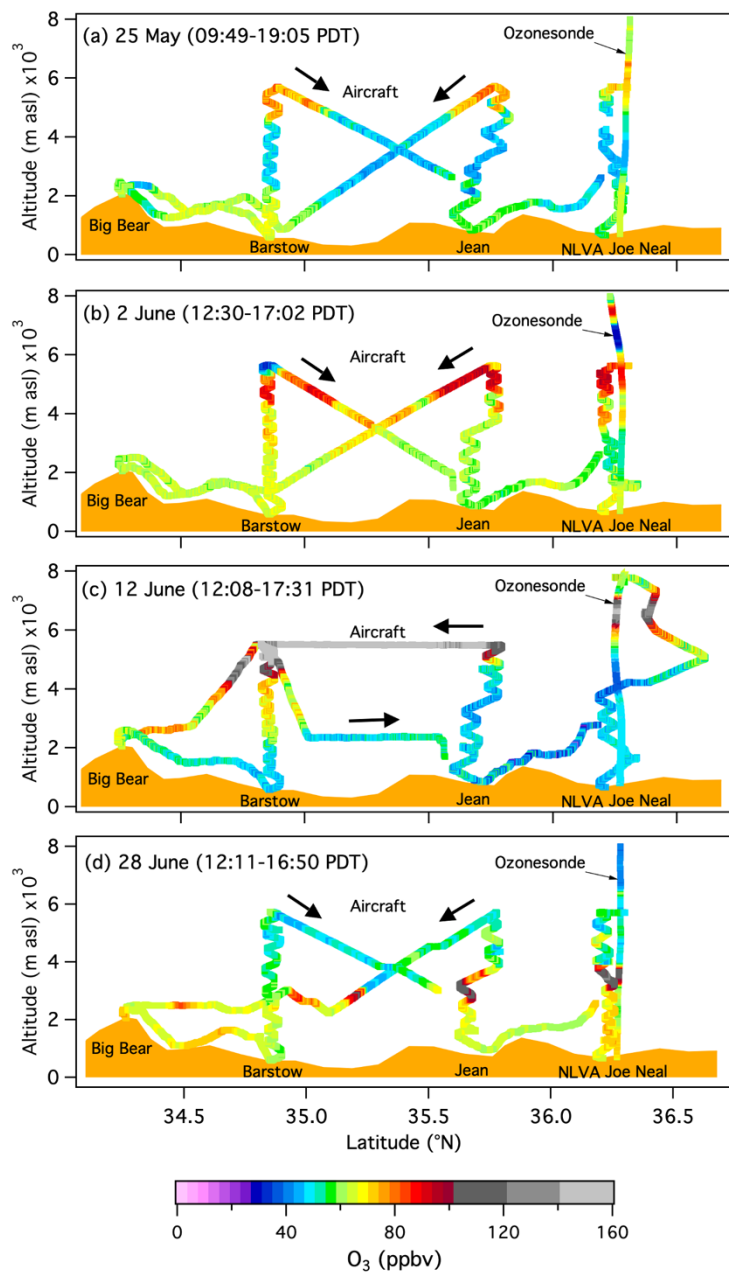


Figure 16: Ozone mixing ratios measured by the ozonesonde and aircraft on the flights to and from Big Bear on: (a) 25 May, (b) 2 June, (c) 12 June, and (d) 28 June. The TOPAZ measurements and AP aircraft profiles are omitted for clarity, as are the Jean and NLVA aircraft profiles from the return legs. The terrain profile is approximate.

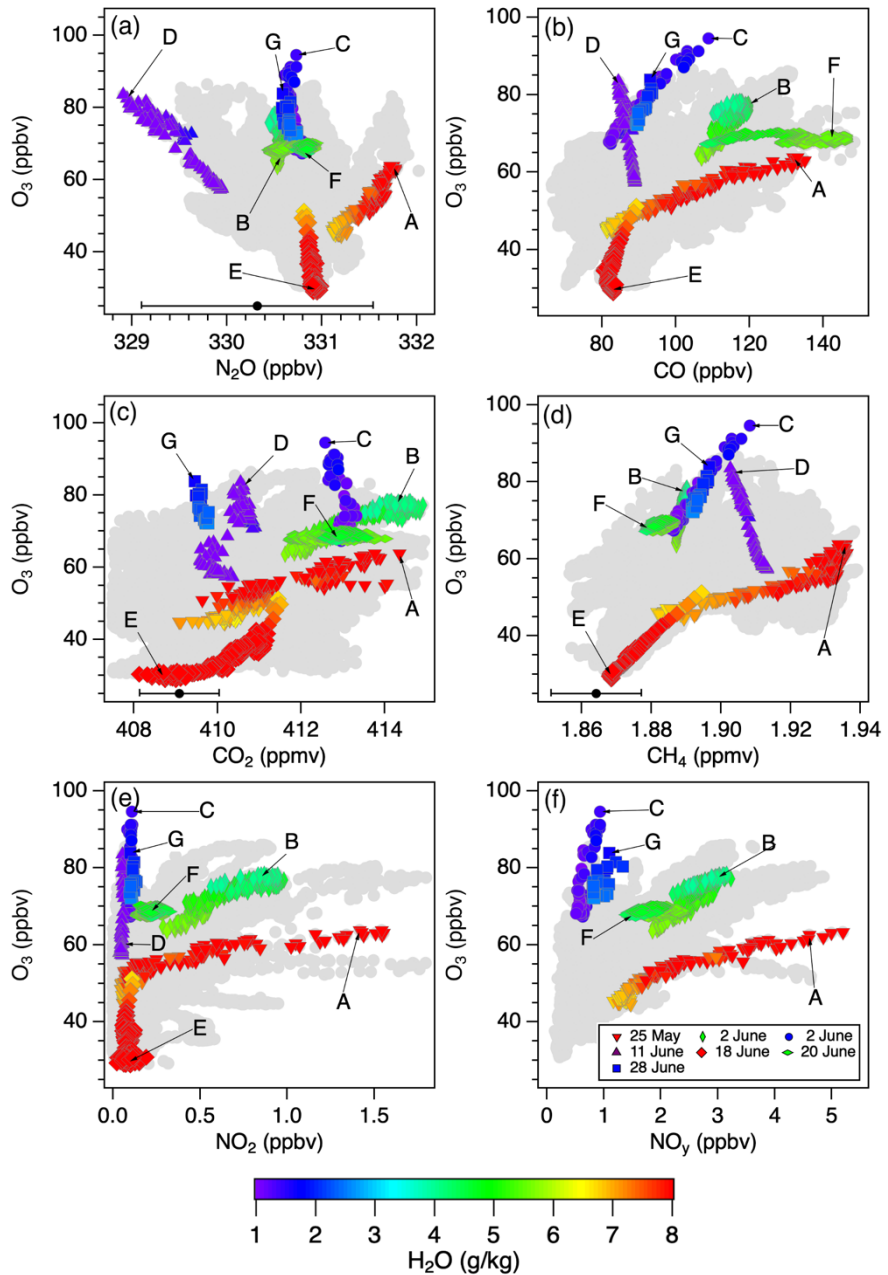


Figure 17: Scatter plots showing the relationships between O₃ and the (a) N₂O, (b) CO, (c) CO₂, (d) CH₄, (e) NO₂, and (f) NO_y tracers on AP during episodes A-G. The gray points show all of the FAST-LVOS measurements. The black points with error bars in (a), (c), and (d) represent the mean ($\pm 1\sigma$) June 2017 concentrations from the NOAA GML Mauna Loa Observatory.

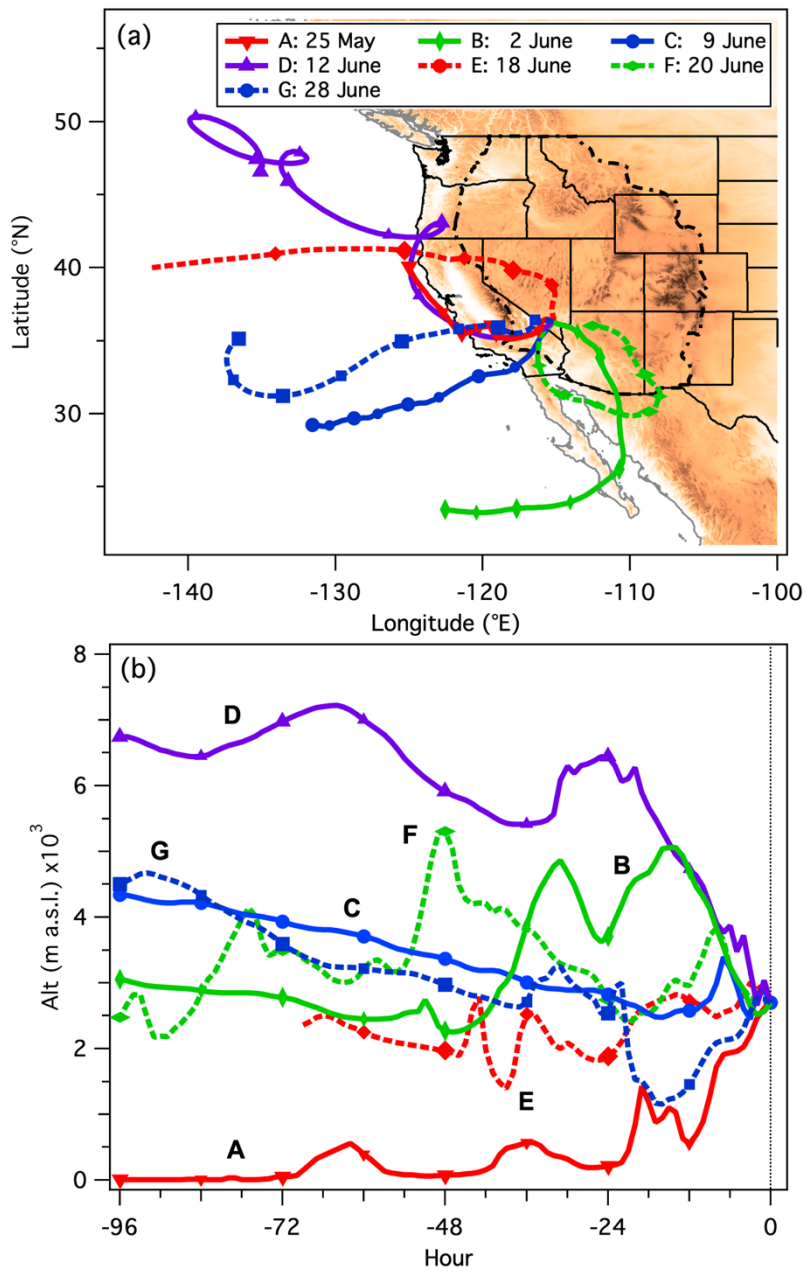


Figure 18: NOAA HYSPLIT 96-h back trajectories launched 2 km above North Las Vegas during episodes A-G. The small and large filled symbols are spaced at 12 and 24 hours apart, respectively. The trajectories were calculated using the 40 km NCEP Eta Data Assimilation System (EDAS) meteorology.

705 Fig. 14 shows that the winds on the summit of AP were mostly southerly during the morning and early afternoon of 28 June, and the mobile laboratory sampled air with much lower O₃ concentrations than that profiled by the lidar. The winds briefly rotated to the northwest in the early evening and the mobile laboratory recorded a drop in relative humidity and increase in O₃ around 1830 PDT (episode G). The relationships in Fig. 17 suggest that this spike was caused by Asian pollution, a conclusion supported by the HYSPLIT back trajectory (dashed blue line) in Fig. 18 which descends from the upper 710 troposphere over the Pacific Ocean before passing over the SJV well above the boundary layer. Although the transient peak in Fig. 6 was detected more than 6 hours after the O₃ layer was entrained, it does support the conclusion that Asian pollution was present in the vicinity of AP on 28 June.

7 Other transport examples

715 Not all of the interesting transport episodes occurred during one of the four IOPs, and the labels C, E, and F in Figs. 6, 17, and 18 highlight three other examples. Fig. 6a shows that the highest 1-min O₃ concentrations (\approx 95 ppbv) measured on AP during *FAST-LVOS* 2017 were sampled during episode C around 0200 PDT on the morning of 9 June. The high O₃ lasted for about an hour, but occurred several hours after TOPAZ had ceased operations for the night. However, the 8 June curtain 720 plot in Fig. 4d shows a 1 km deep layer of high O₃ just above the top of the boundary layer throughout the observing session that appears to have persisted through the night and into the next morning when the lidar operations resumed. The unusual dryness of the air sampled on AP and relationships between O₃ and the other measured species (Fig. 17) suggests that this 725 layer was also Asian pollution that recently descended from the upper troposphere. The episode C measurements completely overlap with the measurements from 28 June (episode G) in many of the scatter plots, suggesting a common origin. The HYSPLIT trajectories in Fig. 18 are also similar, and the peak concentrations measured by TOPAZ, \approx 105 ppbv on 8 June and \approx 115 ppbv on 28 June, are also comparable.

730 The 1-min mobile laboratory measurements from the morning of 18 June (Episode E) include both the highest H₂O (12 g kg⁻¹) and lowest O₃ concentrations (29 ppbv) measured on AP during *FAST-LVOS* 2017. Fig. 4f shows that TOPAZ also measured unusually low O₃ throughout the tropospheric column. As noted above, this episode is attributed to transport of clean marine air deep into the IMW by the anticyclonic flow around the subtropical ridge (Fig. 3e) and the HYSPLIT back 735 trajectory (Fig. 18, dashed red line) suggests that this moist background air was lifted into the lower free tropospheric above the Pacific Ocean more than 4 days earlier, and Figs. 6 and 17 show that the mobile laboratory also measured very low O₃, CO, CO₂, CH₄, and NO₂ concentrations on AP (the NO_y converter was offline). The filled black circles in Fig. 17 show that the O₃, N₂O, CO₂ and CH₄ concentrations measured at AP on the morning of 18 June were comparable to the mean ($\pm 1\sigma$) June 2017 values measured at the high elevation NOAA GML Mauna Loa Observatory (<https://gml.noaa.gov/dv/data/>, last access 16 August 2021). These measurements are thought to represent the background concentrations in the free tropospheric air reaching the U.S. West Coast.

The final example (episode F) coincides with the highest backscatter (Fig. 5f) measured above the NLVA during *FAST-LVOS* 740 2017. These measurements were made about 24 hours after the start of the Holcomb Fire near Big Bear on the afternoon of 19 June (cf. Fig. 1). This fire grew rapidly, but was battled aggressively and the expansion checked at ≈ 600 ha (745 ≈ 1500 acres) by the evening of 21 June. The anticyclonic path followed by the HYSPLIT trajectory (dashed green line) in Fig. 18 passed directly over the Holcomb Fire, and possibly over older fires in Arizona and northern Mexico. The curtain plots in Figs. 4f and 5f show that there was ≈ 85 ppbv of O_3 in the smoke that appeared at ≈ 3 km a.g.l. on the morning of 20 June, but only ≈ 50 ppbv of O_3 in the denser smoke that appeared between 4 and 6 km a.g.l. in the afternoon and evening. Some of the smoke from the second plume was entrained by the convective boundary layer and the CO time series from the mobile laboratory on AP shows a corresponding rise to more than 140 ppbv. However, Fig. 17e shows that there was little NO₂ in the second plume, which is consistent with the absence of any O_3 enhancement in either the sampled air or the lidar measurements.

750

8 Baseline ozone during *FAST-LVOS*

The top five panels of Fig. 19 show the hourly-averaged and MDA8 O_3 measurements from the remote sampling sites operated by the WMRC and the NVDEP during *FAST-LVOS*. All of these sites are located well away from populated areas with the WMRC located ≈ 310 km WNW of the LVV and the NVDEP monitors located between 180 and 250 km to the 755 north (cf. Fig. 1). The bottom panel shows the measurements from the monitor maintained by the CCDAQ in the town of Mesquite ≈ 120 km NE of Las Vegas near the Nevada-Utah border. MDA8 O_3 concentrations exceeding 65 and 70 ppbv are highlighted in orange and red, respectively. The mean MDA8 O_3 mixing ratio ($\pm 1\sigma$, the standard deviation of the mean) is shown in each plot. These measurements show a pronounced elevation trend consistent with descent of O_3 from the free troposphere and destruction at the surface. The former is reflected in the higher mean values and episodic increases at the 760 higher elevations, and the latter in the low night time values at the lower elevations.

The WMRC operates the highest elevation long-term O_3 monitors in the continental U.S., with both the WMS (4.34 km a.s.l.) and BCO (3.88 km a.s.l.) located roughly 1 km higher than the CASTNET site in Gothic, CO (2.93 km a.s.l.), which is the highest regulatory O_3 monitor in the U.S. The MDA8 O_3 measured at the WMS exceeded the 2015 NAAQS of 70 ppbv 765 on 17 of the 46 *FAST-LVOS* sampling days, with a mean MDA8 O_3 of 68 ± 12 ppbv between 15 May and 30 June when there were persistent O_3 layers aloft, and 73 ± 11 ppbv between 23 May and 14 June, the 22-day interval bracketing the beginning of the first and end of the third IOPs. High O_3 was measured during each of the four IOPs with the 1-hour peak concentrations exceeding 100 ppbv on 16 May, 25-26 May, and 9-10 June. The MDA8 O_3 was greater than 65 ppbv on 24 days, including 18 of the 22 days between 23 May and 14 June, and the 4MDA8 O_3 for the 6-week period was 86 ppbv. The 770 MDA8 O_3 concentrations were similar, but about 8 ppbv lower on average at the BCO.

The mean MDA8 O₃ at WSSU, the highest elevation NVDEP site at 2.3 km a.s.l., was about 17 ppbv lower than that at WMS with a 4MDA8 O₃ of 61 ppbv. The large episodic increases measured by the WMRC monitors during the IOPs did not reach the lower lying NVDEP sites, and there were no NAAQS exceedances by any of these non-regulatory monitors.

775 Nevertheless, the mean MDA8 O₃ at these three remote sites ranged from \approx 50 to 55 ppbv, or 70-80% of the NAAQS

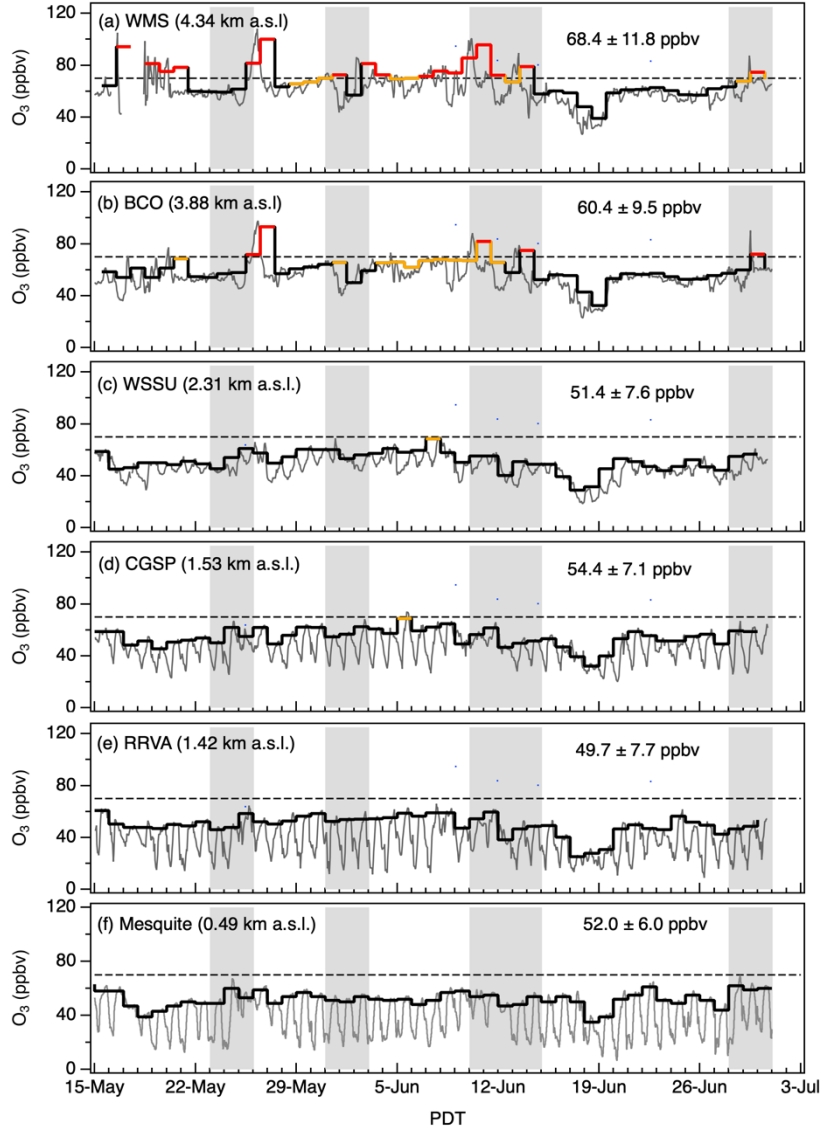


Figure 19: Time series of the 1-h average (gray line) and MDA8 O₃ (black staircase) measurements from the remote monitoring sites. The monitor elevations are shown in parentheses. (a) White Mountain Summit, (b) Barcroft Observatory, (c) Warm Springs Summit, (d) Cathedral Gorge State Park, (e) Railroad Valley, and (f) Mesquite. MDA8 O₃ concentrations exceeding the 2015 NAAQS of 70 ppbv (dashed line) and a potential NAAQS of 65 ppbv are highlighted in red and orange, respectively. The gray bands show the four IOPs. The mean concentrations ($\pm 1\sigma$) are calculated from the 15 May to 30 June MDA8 O₃ measurements.

780

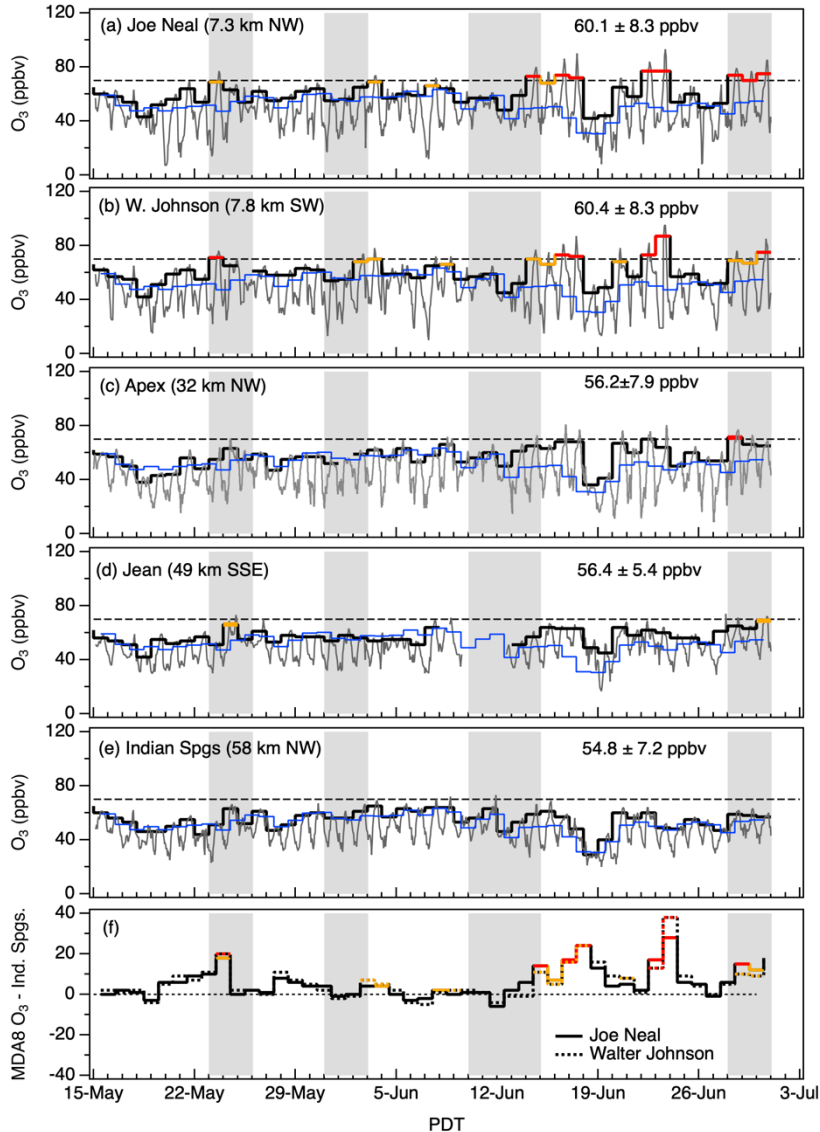
between mid-May and the end of June, with 4MDA8 O₃ concentrations ranging from 59 to 62 ppbv (84-88% of the NAAQS). An earlier analysis of springtime (March-May) measurements from 2012 and 2013 at CGSP (Fine et al., 2015a) 785 found very similar mean MDA8 O₃ concentrations of 51±6 and 50±8 ppbv, respectively. These measurements are comparable to the background (*i.e.*, formed from natural sources plus anthropogenic sources in countries outside the U.S.) monthly mean springtime MDA8 O₃ concentration of 50 ppbv estimated by *Lin et al.* (2012a, 2012b) for higher elevations in the IMW using the GFDL AM3 model for the year 2010, but are significantly higher than the mean MDA8 O₃ of 40±7 ppbv 790 derived by *Zhang et al.* (2011) using GEOS-Chem model runs for the years 2006-2008, and the upper limit of 40-45 ppbv the seasonal mean MDA8 estimated by *Dolwick et al.* (2015) using Community Multiscale Air Quality (CMAQ) and Comprehensive Air Quality Model with Extensions (CAMx) runs for the year 2007. These differences should be viewed with caution since they do not account for changes in Asian precursor emissions or differences in trans-Pacific pollution transport and STT caused by the position of the jet stream (Lin et al., 2015; Albers et al., 2018; Breeden et al., 2021).

795 9 Implications for air quality attainment

The EPA has designated Las Vegas, Nevada a marginal nonattainment area for O₃ 800 (<https://www3.epa.gov/airquality/greenbook/jnc.html>, last access 16 August 2021). The warm and sunny conditions that lead to rapid photochemical production of O₃ also drive the upslope flow into the Spring Mountains that causes O₃ and other pollutants to accumulate in the north-western LVV. The highest O₃ concentrations are usually measured at the Joe Neal (C75) and Walter Johnson (C71) monitors (cf. Fig. 1), which had 2017 ozone design values, *i.e.*, the 3-year running average of the 4th highest MDA8 O₃, of 74 and 72 ppbv, respectively. Fig. 20 plots the hourly-averaged and MDA8 O₃ measurements from these two sites during *FAST-LVOS*, along with the corresponding measurements from the Apex (C22), Jean (1019), and Indian Springs (C7772) monitors (cf. Fig. 1). The thin blue line in each plot represents the average of the RRVA, CGSP, and WSSU MDA8 O₃ measurements from Fig. 19, which we use as an estimate for the southern Nevada mean baseline 805 MDA8 O₃. The Joe Neal and Walter Johnson monitors also recorded the highest O₃ concentrations in Clark County during *FAST-LVOS*, and exceeded the 2015 NAAQS on 7 and 6 days, respectively. Most of these exceedances coincided with the higher temperatures that followed the poleward expansion of the subtropical ridge in mid-June (cf. Fig. S1). Several of the other monitors located within a 15 km radius of the NLVA also exceeded the NAAQS on at least one of these days. There 810 was only one exceedance each at the slightly more distant Apex (32 km NE) and Green Valley (22 km SE) monitors, and no exceedances at the Boulder City (40 km SE), Jean (49 km SSE), or Indian Springs (58 km NW) monitors (cf. Fig. 1c). Note that the Jean monitor was offline from 9-12 June. All of the CCDEQ monitors measured unusually low O₃ on 18-19 June.

The MDA8 O₃ measured by the Indian Springs monitor was very similar to the NVDEP baseline values, with the largest 815 differences arising on 16-17 June when the anticyclonic marine incursion had reached the more northerly NVDEP sites, but had not yet reached Clark County. The mean NVDEP and Indian Springs time series agree to within 3% on average

$(R^2=0.69)$ if the measurements from these two days are excluded. This suggests that the Indian Springs measurements may be a good proxy for the LVV baseline O_3 during the *FAST-LVOS* campaign, and the solid black line in Fig. 20f represents



820 **Figure 20:** Time series of the 1-h (gray line) and MDA8 (black staircase) O_3 measurements from the CCDAQ (a) Joe Neal, (b) Walter Johnson, (c) JD Smith, (d) Jean, and (e) Indian Springs monitors. The distances from the NLVA are shown in parentheses. Note that the Jean monitor was offline June 9-12. The blue lines show the baseline MDA8 O_3 estimated from the mean of the NVDEP measurements. The bottom panel (f) plots the differences between the Indian Springs monitor and the Joe Neal (solid) and Walter Johnson (dotted) monitors. MDA8 O_3 concentrations exceeding the 2015 NAAQS of 70 ppbv (dashed line) and a potential NAAQS of 65 ppbv are highlighted in red and orange, respectively. The gray bands show the four IOPs. The mean concentrations ($\pm 1\sigma$) are calculated from the 15 May to 30 June MDA8 measurements.

the difference between the Joe Neal MDA8 O₃ concentrations and the Indian Springs monitor. The dotted line is similar, but shows the difference for the Walter Johnson monitor. The measurements from days where the MDA8 O₃ concentrations exceeded 65 or 70 ppbv are highlighted as before. The MDA8 O₃ concentrations at Joe Neal and Walter Johnson were significantly higher than the baseline concentrations on 23 May, with the Walter Johnson and Joe Neal monitors reaching 71 and 69 ppbv, respectively. Although the lidar, aircraft, and ozonesonde observations showed high O₃ aloft throughout the first IOP, there was no obvious mixing of the high O₃ into the boundary layer. There were multiple exceedances in the San Joaquin Valley and South Coast Air Basins on 22-24 May, however, and the elevated O₃ in the LVV on 23 May is most likely due to regional transport and local production (cf. Section 6.1). Ozone was also elevated in the LVV on 2-3 June, and the measurements in Fig. 12 do appear to show entrainment of stratospheric O₃ and Asian pollution into the boundary layer although this supposition could not be confirmed by the AP measurements. The MDA8 O₃ reached 68 and 65 ppbv, respectively, at Walter Johnson and Joe Neal on 2 June, and 70 and 69 ppbv on 3 June. The descending O₃ may also have contributed to an isolated cluster of NAAQS exceedances at state and tribal monitors in southwestern Colorado and northwestern New Mexico, and to the MDA8 O₃ of 70 ppbv recorded at Mesa Verde National Park on 3 June.

840

The high winds (>20 m s⁻¹ at the surface) preceding the major intrusion event of 11-13 June (IOP3) cleared local pollution out of the LVV ahead of the descending stratospheric air and the MDA8 O₃ concentrations at Walter Johnson and Joe Neal reached only 59 and 57 ppbv on 11 June. Interestingly, the highest reported MDA8 O₃ concentrations in Clark County on that day were 63 and 60 ppbv at Indian Springs and Apex, respectively. There were multiple NAAQS exceedances in 845 Arizona on 13-15 June, however, including an MDA8 O₃ concentration of 91 ppbv measured on 14 June about 60 km northeast of Phoenix at the Tonto National Monument. The GFDL-AM4 model estimated 20-30 ppbv MDA8 O₃ enhancements from stratospheric influence around this site and other areas in Arizona on June 14 (see Fig. 9 in Zhang et al., 2020). The next highest values recorded at this site in 2017 were 78 ppbv on 15 June and 77 ppbv on 13 June.

850

The Walter Johnson and Joe Neal measurements in Fig. 20 appear qualitatively very different from the White Mountain Summit and Barcroft Observatory measurements in Fig. 19. Nearly all of the NAAQS exceedances at the high elevation sites occurred before the middle of June when stratospheric intrusions and Asian pollution plumes appeared frequently in the middle and lower troposphere, but nearly all of the exceedances in the LVV occurred after the middle of June when higher temperatures and stagnant conditions increased photochemical production of O₃ in the boundary layer. The high 855 temperatures also exacerbated regional wildfires, including the Holcomb and Brian Head fires whose plumes reached the LVV in the third week of June (cf. Figs. 4f and 5f). Note that these fires did not increase surface O₃ at the Jean, Indian Springs, or Mesquite monitors, suggesting that the smoke plumes were NO_x-limited and significant O₃ production required additional NO_x from urban sources in the LVV (Singh et al., 2012). High O₃ was measured both in and above the boundary layer on the last three days of June during IOP4, with a clear example showing the entrainment of a fine-scale Asian 860 pollution plume by the growing convective boundary layer on 28 June. This event contributed to MDA8 O₃ of 69 and 74

ppbv at Walter Johnson and Joe Neal, as well as the only exceedance by the Apex monitor which measured 71 ppbv. The high elevation WMRC monitors also measured elevated O₃ in the lower free troposphere on 29 June, and some of this O₃ may have contributed to the exceedances in the LVV on that day.

865 The 2013 LVOS and 2017 *FAST*-LVOS campaigns were conducted over the same late spring/early summer time period, but the distribution and sources of the high O₃ measured in Clark County during 2013 and 2017 were very different. The MDA8 O₃ exceeded 70 ppbv at one or more of the Clark County monitors on 17 days in May and June of 2013, but only 8 days in May and June of 2017. In 2013, 12 of the 17 exceedance days occurred *before* 13 June, and 9 were in May. In 2017, 7 of the 8 exceedance days occurred *after* 13 June with only one in May. Only one of the high O₃ events in 2017 affected more than 870 4 of the 12 active monitors, but 8 of the 17 high O₃ events in 2013 affected 4 of the 11 active monitors, and 4 affected 9 or more of the CAMS. These were the stratospheric intrusion/wildfire event of 4-5 May (Langford et al., 2015a), stratospheric intrusion events of 21 and 25 May (Langford et al., 2018), and Asian pollution event of 21 June (Langford et al., 2017). These major events affected monitors outside of Las Vegas as well as those in the valley and the Jean monitor exceeded 70 ppbv on 8 days in 2013, but not once in 2017 (the Indian Springs monitor was not installed until 2015).

875

10 Summary and conclusions

The 6-week long *FAST*-LVOS field campaign collected a wealth of lidar, surface, aircraft, and ozonesonde measurements that greatly improve our understanding of O₃ transport in Clark County, Nevada and the greater Southwestern U.S. and Intermountain West in late spring and early summer. Daily lidar observations found high O₃ layers in the lower and middle 880 free troposphere above Las Vegas on more than 75% (35 of 45) of the measurement days. The highest tropospheric concentrations were measured on 11-12 June when both the lidar and an ozonesonde launched nearby found up to 250 ppbv within 5.5 km of the surface. Several of these elevated O₃ layers were also sampled by a high elevation research monitor located more than 300 km to the west-northwest in the White Mountains of California (Burley and Bytnerowicz, 2011) and the MDA8 O₃ concentrations at this site averaged more than 68 ppbv over the course of the study. Simulations from the 885 FLEXPART, GEOS-Chem, and AM4 models (Zhang et al., 2020) show that the elevated layers were created by stratospheric intrusions or long-range transport from Asia, and in most cases, a mixture of the two. Aircraft measurements made during the four IOPs support this conclusion, and the aircraft mapped the spatial distribution of these plumes above the Mojave Desert in Southern Nevada and California. *FAST*-LVOS also documented several fine-scale anticyclonic streamers in addition to the deep cyclonic intrusions that are the focus of most studies.

890

The *FAST*-LVOS measurements also captured several examples of O₃ being entrained from aloft by the convective boundary layer, and correlations between the different tracers measured on AP (2.7 km a.s.l.) showed the distinctive signatures of both stratospheric air and Asian pollution on multiple occasions. The AP measurements also found wildfire influences and evidence for regional transport of anthropogenic pollution from the San Joaquin Valley in addition to local upslope transport

895 of pollution from the LVV. Although none of the stratospheric intrusions or Asian pollution events *directly* caused any of the
NAAQS exceedances in the LVV during *FAST-LVOS*, they clearly added to the surface concentrations on at least one (14
June) of the exceedance days and contributed to the mean MDA8 O₃ of 50-55 ppbv measured at the remote sites in rural
Nevada during the study. These mean baseline concentrations represent 70-80% of the 2015 NAAQS of 70 ppbv, making it
more difficult for Western air quality managers to maintain surface O₃ concentrations below the NAAQS in the IMW during
900 late spring and early summer (Cooper et al., 2015; Uhl and Moore, 2018).

Data availability. FLEXPART simulations presented in this paper are available upon request to the corresponding author
(andrew.o.langford@noaa.gov). Field measurements during *FAST-LVOS* are available at
<https://www.esrl.noaa.gov/csd/projects/fastlvos> (last access: 16 August 2021; NOAA, 2021).

905 *Supplement.* The supplement related to this article is available online at:

Author contributions. AOL and CJS conceived this study and planned the field campaign; AOL, CJS, RJA, SPS, AMW, IP,
PDC, CWS, JP, TBR, SSB, ZD, GK, SC, and DJC prepared the instruments and carried out the field measurements; SB and
TAB analyzed the Doppler lidar data and KCA compiled and archived the mobile laboratory measurements; LZ performed
910 the GFDL-AM4 simulations and all analysis under the supervision of ML; RBP and MP conducted the RAQMS and RAP-
Chem model forecasts, respectively; JB and SE executed the FLEXPART model calculations; AOL did the analyses and
wrote the article with inputs from all coauthors.

Competing interests. The authors declare that they have no conflict of interest.

Disclaimer. The scientific results and conclusions, as well as any views or opinions expressed herein, are those of the
author(s) and do not necessarily reflect the views of NOAA or the Department of Commerce.

915 *Acknowledgements.* We would like to thank Zheng Li and Rodney Langston of CCDAQ for their support and assistance in
the planning and execution of the project, Paul Fransioli for providing the wind profiler and visibility camera data, and
various other CCDAQ personnel who provided logistical support during the execution of the field campaign. We would also
like to thank Sheryl Fontaine and Daren Winkelman from the Nevada Division of Environmental Protection Bureau of
920 Air Quality Planning for providing the Railroad Valley, Warm Springs Summit, and Cathedral Gorge State Park
measurements. We are most grateful to Zaheer Kamal for his able piloting of the SA Mooney aircraft. We would also like to
thank Richard Marchbanks for his assistance during the field campaign and Cathy Burgdorf-Rasco for maintaining the
FAST-LVOS data site. Finally, we would also like to thank Dr. K. E. Knowland and an anonymous reviewer for their careful
reading of the manuscript and helpful suggestions.

925 *Financial support.* The Fires, Asian, and Stratospheric Transport-Las Vegas Ozone Study (*FAST-LVOS*) field measurements and model simulations were funded by the Clark County Department of Air Quality (CCDAQ) under contracts CBE 604318-16 and CBE 605334-19 (NOAA CCSL), CBE 603380-17 (Scientific Aviation), and CBE 604279-16 (NOAA GFDL). The NOAA CSL lidar operations were also supported by the NOAA Climate Program Office, Atmospheric Chemistry, Carbon Cycle, and Climate (AC4) Program and the NASA-sponsored Tropospheric Ozone Lidar Network (TOLNet, <http://www-air.larc.nasa.gov/missions/TOLNet/>, last access 16 August 2021)

930 **References**

Albers, J. R., Perlwitz, J., Butler, A. H., Birner, T., Kiladis, G. N., Lawrence, Z. D., Manney, G. L., Langford, A. O., and Dias, J.: Mechanisms Governing Interannual Variability of Stratosphere-to-Troposphere Ozone Transport, *J. Geophys. Res.-Atmos.*, 123, 234-260, 10.1002/2017jd026890, 2018.

Albers, J. R., Butler, A. H., Breedon, M. L., Langford, A. O., and Kiladis, G. N.: Subseasonal prediction of springtime Pacific–North American transport using upper-level wind forecasts, *Weather Clim. Dynam.*, 2, 433-452, 10.5194/wcd-2-433-2021, 2021.

Alvarez II, R. J., Brewer, W. A., Law, D. C., Machol, J. L., Marchbanks, R. D., Sandberg, S. P., Senff, C. J., and Weickmann, A. M.: Development and Application of the TOPAZ Airborne Lidar System by the NOAA Earth System Research Laboratory, 24th International Laser Radar Conference, Boulder, Colorado, USA, 2008, 68-71,

940 Ancellet, G., Beekmann, M., and Papayannis, A.: Impact of a cutoff low development on downward transport of ozone in the troposphere, *J. Geophys. Res.*, 99, 3451-3468, 1994.

Appenzeller, C., and Davies, H. C.: Structure of stratospheric intrusions into the troposphere, *Nature*, 358, 570-572, 1992.

Appenzeller, C., Davies, H. C., and Norton, W. A.: Fragmentation of stratospheric intrusions, *J. Geophys. Res.-Atmos.*, 101, 1435-1456, Doi 10.1029/95jd02674, 1996.

945 Assonov, S. S., Brenninkmeijer, C. A. M., Schuck, T., and Umezawa, T.: N₂O as a tracer of mixing stratospheric and tropospheric air based on CARIBIC data with applications for CO₂, *Atmospheric Environment*, 79, 769-779, 10.1016/j.atmosenv.2013.07.035, 2013.

Bonasoni, P., Evangelisti, F., Bonafe, U., Ravagnani, F., Calzolari, F., Stohl, A., Tositti, L., Tubertini, O., and Colombo, T.: Stratospheric ozone intrusion episodes recorded at Mt. Cimone during the VOTALP project: case studies, *Atmospheric Environment*, 34, 1355-1365, 2000.

950 Bonin, T. A., Carroll, B. J., Hardesty, R. M., Brewer, W. A., Hajny, K., Salmon, O. E., and Shepson, P. B.: Doppler Lidar Observations of the Mixing Height in Indianapolis Using an Automated Composite Fuzzy Logic Approach, *Journal of Atmospheric and Oceanic Technology*, 35, 473-490, 10.1175/Jtech-D-17-0159.1, 2018.

Breeden, M. L., Butler, A. H., Albers, J. R., Sprenger, M., and Langford, A. O.: The spring transition of the North Pacific jet
955 and its relation to deep stratosphere-to-troposphere mass transport over western North America, *Atmospheric Chemistry and Physics*, 21, 2781-2794, 10.5194/acp-21-2781-2021, 2021.

Brioude, J., Cooper, O. R., Trainer, M., Ryerson, T. B., Holloway, J. S., Baynard, T., Peischl, J., Warneke, C., Neuman, J. A.,
de Gouw, J., Stohl, A., Eckhardt, S., Frost, G. J., McKeen, S. A., Hsie, E.-Y., Fehsenfeld, F. C., and Nédélec, P.:
Mixing between a stratospheric intrusion and a biomass burning plume, *Atmos. Chem. Phys.*, 7, 4229-4235, 2007.

960 Brioude, J., Cooper, O. R., Feingold, G., Trainer, M., Freitas, S. R., Kowal, D., Ayers, J. K., Prins, E., Minnis, P., McKeen,
S. A., Frost, G. J., and Hsie, E. Y.: Effect of biomass burning on marine stratocumulus clouds off the California
coast, *Atmos. Chem. Phys.*, 9, 8841-8856, 2009.

Browell, E. V., Danielsen, E. F., Ismail, S., Gregory, G. L., and Beck, S. M.: Tropopause fold structure determined from
airborne lidar and in situ measurements, *J. Geophys. Res.*, 92, 2112-2120, 1987.

965 Brown-Steiner, B., and Hess, P.: Asian influence on surface ozone in the United States: A comparison of chemistry,
seasonality, and transport mechanisms, *J. Geophys. Res.*, 116, 10.1029/2011JD015846, 2011.

Burley, J. D., and Bytnerowicz, A.: Surface ozone in the White Mountains of California, *Atmospheric Environment*, 45,
4591-4602, 10.1016/j.atmosenv.2011.05.062, 2011.

970 Clark, H., Sauvage, B., Thouret, V., Nedelec, P., Blot, R., Wang, K. Y., Smit, H., Neis, P., Petzold, A., Athier, G.,
Boulanger, D., Cousin, J. M., Beswick, K., Gallagher, M., Baumgardner, D., Kaiser, J., Flaud, J. M., Wahner, A.,
Volz-Thomas, A., and Cammas, J. P.: The first regular measurements of ozone, carbon monoxide and water vapour
in the Pacific UTLS by IAGOS, *Tellus Series B-Chemical and Physical Meteorology*, 67,
10.3402/tellusb.v67.28385, 2015.

975 Coggon, M. M., Veres, P. R., Yuan, B., Koss, A., Warneke, C., Gilman, J. B., Lerner, B. M., Peischl, J., Aikin, K. C.,
Stockwell, C. E., Hatch, L. E., Ryerson, T. B., Roberts, J. M., Yokelson, R. J., and de Gouw, J. A.: Emissions of
nitrogen-containing organic compounds from the burning of herbaceous and arboraceous biomass: Fuel
composition dependence and the variability of commonly used nitrile tracers, *Geophysical Research Letters*, 43,
9903-9912, 10.1002/2016gl070562, 2016.

980 Colette, A., and Ancellet, G.: Variability of the tropospheric mixing and of streamer formation and their impact on the
lifetime of observed ozone layers, *Geophys. Res. Lett.*, 33, L09808, doi:09810.01029/02006GL025793,
10.1029/2006gl025793, 2006.

985 Cooper, O. R., C., F., Parrish, D. D., Trainer, M., Dunlea, E., Ryerson, T. B., Hubler, G., Fehsenfeld, F. C., Nicks, D.,
Holloway, J. S., Nowak, J., Brock, C., de Gouw, J., Warneke, C., Roberts, J. M., Flocke, F., and Moody, J.: A case
study of trans-Pacific warm conveyor belt transport: The influence of merging airstreams on trace gas import to
North America, *J. Geophys. Res.*, 108, 10.1029/2003JD003624, 2004.

Cooper, O. R., Langford, A. O., Parrish, D. D., and Fahey, D. W.: Challenges of a lowered US ozone standard, *Science*, 348,
1096-1097, 10.1126/science.aaa5748, 2015.

Danielsen, E. F.: Project Springfield Report, Defense Atomic Support Agency, Washington, D.C.DASA 1517, 1964.

Delmas, R.: An overview of present knowledge on methane emission from biomass burning, *Fertilizer research*, 37, 181-190, 10.1007/BF00748936, 1994.

Dolwick, P., F. Akhtar, K. R. Baker, N. Possiel, H. Simon, and G. Tonnesen (2015), Comparison of background ozone estimates over the western United States based on two separate model methodologies, *Atmospheric Environment*, 109, 282-296, doi:10.1016/j.atmosenv.2015.01.005.

Duncan, B. N., Malings, C. A., Knowland, K. E., Anderson, D. C., Prados, A. I., Keller, C. A., Cromar, K. R., Pawson, S., and Ensz, H.: Augmenting the Standard Operating Procedures of Health and Air Quality Stakeholders With NASA Resources, *Geohealth*, 5, ARTN e2021GH000451, doi:10.1029/2021GH000451, 2021.

Eisele, H., Scheel, H. E., Sladkovic, R., and Trickl, T.: High-resolution lidar measurements of stratosphere-troposphere exchange, *Journal of the Atmospheric Sciences*, 56, 319-330, Doi 10.1175/1520-0469(1999)056<0319:Hrlmos>2.0.Co; 2, 1999.

EPA: Integrated Science Assessment of Ozone and Related Photochemical Oxidants (Final Report), United States Environmental Protection Agency, Research Triangle Park, NC, 2013.

EPA: Policy Assessment for the Review of the Ozone National Ambient Air Quality Standards. Final Report, United States Environmental Protection Agency, Research Triangle Park, NC, 2014.

Faloona, I. C., Chiao, S., Eiserloh, A. J., Alvarez, R. J., Kirgis, G., Langford, A. O., Senff, C. J., Caputi, D., Hu, A., Iraci, L. T., Yates, E. L., Marrero, J. E., Ryoo, J. M., Conley, S., Tanrikulu, S., Xu, J., and Kuwayama, T.: The California Baseline Ozone Transport Study (CABOTS), *Bulletin of the American Meteorological Society*, 101, E427-E445, 10.1175/Bams-D-18-0302.1, 2020.

Fine, R., Miller, M. B., Burley, J., Jaffe, D. A., Pierce, R. B., Lin, M. Y., and Gustin, M. S.: Variability and sources of surface ozone at rural sites in Nevada, USA: Results from two years of the Nevada Rural Ozone Initiative, *Sci Total Environ.*, 530, 471-482, 10.1016/j.scitotenv.2014.12.027, 2015a.

Fine, R., Miller, M. B., Yates, E. L., and Gustin, M. S.: Investigating the influence of long-range transport on surface O₃ in Nevada, USA using observations from multiple measurement platforms. , *Sci Total Environ.*, 530-531, 493-504, 10.1016/j.scitotenv.2015.03.125., 2015b.

Gelaro, R., McCarty, W., Suarez, M. J., Todling, R., Molod, A., Takacs, L., Randles, C. A., Darmenov, A., Bosilovich, M. G., Reichle, R., Wargan, K., Coy, L., Cullather, R., Draper, C., Akella, S., Buchard, V., Conaty, A., da Silva, A. M., Gu, W., Kim, G. K., Koster, R., Lucchesi, R., Merkova, D., Nielsen, J. E., Partyka, G., Pawson, S., Putman, W., Rienecker, M., Schubert, S. D., Sienkiewicz, M., and Zhao, B.: The Modern-Era Retrospective Analysis for Research and Applications, Version 2 (MERRA-2), *Journal of Climate*, 30, 5419-5454, 10.1175/Jcli-D-16-0758.1, 2017.

|020 Gustin, M. S., Fine, R., Miller, M., Jaffe, D., and Burley, J.: The Nevada Rural Ozone Initiative (NVROI): Insights to understanding air pollution in complex terrain, *Sci Total Environ.*, 530, 455-470, 10.1016/j.scitotenv.2015.03.046, 2015.

Hamill, P., Iraci, L. T., Yates, E. L., Gore, W., Bui, T. P., Tanaka, T., and Loewenstein, M.: A New Instrumented Airborne Platform for Atmospheric Research, *Bull. Am. Meteorol. Soc.*, 97, 397-404, 10.1175/Bams-D-14-00241.1, 2016.

|025 Hintsa, E. J., Boering, K. A., Weinstock, E. M., Anderson, J. G., Gary, B. L., Pfister, L., Daube, B. C., Wofsy, S. C., Loewenstein, M., Podolske, J. R., Margitan, J. J., and Bui, T. P.: Troposphere-to-stratosphere transport in the lowermost stratosphere from measurements of H₂O, CO₂, N₂O, and O₃, *Geophys. Res. Lett.*, 25, 2655-2658, 1998.

Holloway, T., Levy, H., and Kasibhatla, P.: Global distribution of carbon monoxide, *J. Geophys. Res.-Atmos.*, 105, 12123-12147, Doi 10.1029/1999jd901173, 2000.

|030 Hudman, R. C., Jacob, D. J., Cooper, O. R., Evans, M. J., Heald, C. L., Park, R. J., Fehsenfeld, F., Flocke, F., Holloway, J., Hubler, G., Kita, K., Koike, M., Kondo, Y., Neuman, A., Nowak, J., Oltmans, S., Parrish, D., Roberts, J. M., and Ryerson, T.: Ozone production in transpacific Asian pollution plumes and implications for ozone air quality in California, *J. Geophys. Res.*, 109, 10.1029/2004jd004974, 2004.

Jaffe, D. A., Cooper, O. R., Fiore, A. M., Henderson, B. H., Tonneson, G. S., Russell, A. G., Henze, D. K., Langford, A. O.,|035 Lin, M., and Moore, T.: Scientific assessment of background ozone over the U.S.: Implications for air quality management., *Elem Sci Anth.*, 6, <http://doi.org/10.1525/elementa.309>, 2018.

James, P., Stohl, A., Forster, C., Eckhardt, S., Seibert, P., and Frank, A.: A 15-year climatology of stratosphere-troposphere exchange with a Lagrangian particle dispersion model: 2. Mean climate and seasonal variability *J. Geophys. Res.*, 108, doi:10.1029/2002JD002639, 2003.

|040 Karstadt, M., Callaghan, B., and United States. Environmental Protection Agency. Office of Air and Radiation.: The plain English guide to the Clean Air Act, U.S. Environmental Protection Agency For sale by the U.S. G.P.O., Supt. of Docs., Washington, DC, 28 p. pp., 1993.

Langford, A. O., Masters, C. D., Proffitt, M. H., Hsie, E. Y., and Tuck, A. F.: Ozone measurements in a tropopause fold associated with a cut-off low system, *Geophysical Research Letters*, 23, 2501-2504, Doi 10.1029/96gl02227, 1996.

|045 Langford, A. O., and Reid, S. J.: Dissipation and mixing of a small-scale stratospheric intrusion in the upper troposphere, *J. Geophys. Res.*, 103, 31265-31276, 1998.

Langford, A. O., Senff, C. J., Alvarez, R. J., Banta, R. M., and Hardesty, R. M.: Long-range transport of ozone from the Los Angeles Basin: A case study, *Geophys. Res. Lett.*, 37, L06807, 10.1029/2010gl042507, 2010.

|050 Langford, A. O., Brioude, J., Cooper, O. R., Senff, C. J., Alvarez, R. J., Hardesty, R. M., Johnson, B. J., and Oltmans, S. J.: Stratospheric influence on surface ozone in the Los Angeles area during late spring and early summer of 2010, *J. Geophys. Res.*, 117, D00V06, 10.1029/2011JD016766, 2012.

Langford, A. O., Pierce, R. B., and Schultz, P. J.: Stratospheric intrusions, the Santa Ana winds, and wildland fires in Southern California, *Geophys. Res. Lett.*, 42, 6091-6097, 10.1002/2015gl064964, 2015a.

Langford, A. O., Senff, C. J., Alvarez, R. J., Brioude, J., Cooper, O. R., Holloway, J. S., Lin, M. Y., Marchbanks, R. D.,
1055 Pierce, R. B., Sandberg, S. P., Weickmann, A. M., and Williams, E. J.: An overview of the 2013 Las Vegas Ozone
Study (LVOS): Impact of stratospheric intrusions and long-range transport on surface air quality, *Atmos. Environ.*,
109, 305-322, 10.1016/J.Atmosenv.2014.08.040, 2015b.

Langford, A. O., Alvarez, R. J., Brioude, J., Fine, R., Gustin, M. S., Lin, M. Y., Marchbanks, R. D., Pierce, R. B., Sandberg,
1060 S. P., Senff, C. J., Weickmann, A. M., and Williams, E. J.: Entrainment of stratospheric air and Asian pollution by
the convective boundary layer in the southwestern U.S, *J. Geophys. Res.*, 122, 1312-1337, 10.1002/2016JD025987,
2017.

Langford, A. O., Alvarez II, R. J., Brioude, J., Evan, S., Iraci, L. T., Kirgis, G., Kuang, S., Leblanc, T., Newchurch, M. J.,
Pierce, R. B., Senff, C. J., and Yates, E. L.: Coordinated profiling of stratospheric intrusions and transported
1065 pollution by the Tropospheric Ozone Lidar Network (TOLNet) and NASA Alpha Jet Atmospheric eXperiment
(AJAX): Observations and comparison to HYSPLIT, RAQMS, and FLEXPART, *Atmos. Environ.*, 174, 1-14,
<https://doi.org/10.1016/j.atmosenv.2017.11.031>, 2018.

Langford, A. O., Alvarez II, R. J., Kirgis, G., Senff, C. J., Caputi, D., Conley, S. A., Faloona, I. C., Iraci, L. T., Marrero, J. E.,
McNamara, M. E., Ryoo, J. M., and Yates, E. L.: Intercomparison of lidar, aircraft, and surface ozone
1070 measurements in the San Joaquin Valley during the California Baseline Ozone Transport Study (CABOTS), *Atmos.*
Meas. Tech., 12, 1889-1904, 10.5194/amt-12-1889-2019, 2019.

Laughner, J. L., and Cohen, R. C.: Direct observation of changing NO_x lifetime in North American cities, *Science*, 366, 723-
+, 10.1126/science.aax6832, 2019.

Leblanc, T., Brewer, M. A., Wang, P. S., Granados-Muñoz, M. J., Strawbridge, K. B., Travis, M., Firanski, B., Sullivan, J. T.,
McGee, T. J., Sumnicht, G. K., Twigg, L. W., Berkoff, T. A., Carrion, W., Gronoff, G., Aknan, A., Chen, G.,
1075 Alvarez, R. J., Langford, A. O., Senff, C. J., Kirgis, G., Johnson, M. S., Kuang, S., and Newchurch, M. J.:
Validation of the TOLNet lidars: the Southern California Ozone Observation Project (SCOOP), *Atmos. Meas.*
Tech., 11, 6137-6162, 10.5194/amt-11-6137-2018, 2018.

Lefohn, A. S., Emery, C., Shadwick, D., Wernli, H., Jung, J., and Oltmans, S. J.: Estimates of background surface ozone
concentrations in the United States based on model-derived source apportionment, *Atmos. Environ.*, 84, 275-288,
1080 10.1016/J.Atmosenv.2013.11.033, 2014.

Lin, M. Y., Fiore, A. M., Cooper, O. R., Horowitz, L. W., Langford, A. O., Levy, H., Johnson, B. J., Naik, V., Oltmans, S. J.,
and Senff, C. J.: Springtime high surface ozone events over the western United States: Quantifying the role of
stratospheric intrusions, *J. Geophys. Res.*, 117, D00v22, 10.1029/2012jd018151, 2012a.

Lin, M. Y., Fiore, A. M., Horowitz, L. W., Cooper, O. R., Naik, V., Holloway, J., Johnson, B. J., Middlebrook, A. M.,
1085 Oltmans, S. J., Pollack, I. B., Ryerson, T. B., Warner, J. X., Wiedinmyer, C., Wilson, J., and Wyman, B.: Transport
of Asian ozone pollution into surface air over the western United States in spring, *J. Geophys. Res.*, 117, D00v07,
10.1029/2011JD016961, 2012b.

Lin, M. Y., Fiore, A. M., Horowitz, L. W., Langford, A. O., Oltmans, S. J., Tarasick, D., and Rieder, H. E.: Climate variability modulates western US ozone air quality in spring via deep stratospheric intrusions, *Nat. Comm.*, 6, 1090 10.1038/Ncomms8105, 2015.

Malicet, J., Daumont, D., Charbonnier, J., Parisse, C., Chakir, A., and Brion, J.: Ozone UV Spectroscopy .2. Absorption Cross-Sections and Temperature-Dependence, *J. Atmos. Chem.*, 21, 263-273, 10.1007/Bf00696758, 1995.

Manney, G. L., and Stanford, J. L.: On the relation of 6.7 μ m water vapour features to isentropic distributions of potential vorticity, *Q.J.R. Meteorol. Soc.*, 113, 1048-1057, 1987.

Nieto, R., Gimeno, L., De La Torre, L., Ribera, P., Gallego, D., Garcia-Herrera, R., Garcia, J. A., Nunez, M., Redano, A., and Lorente, J.: Climatological features of cutoff low systems in the Northern Hemisphere, *Journal of Climate*, 18, 1095 3085-3103, Doi 10.1175/Jcli3386.1, 2005.

Peischl, J., Ryerson, T. B., Holloway, J. S., Trainer, M., Andrews, A. E., Atlas, E. L., Blake, D. R., Daube, B. C., Dlugokencky, E. J., Fischer, M. L., Goldstein, A. H., Guha, A., Karl, T., Kofler, J., Kosciuch, E., Misztal, P. K., Perring, A. E., Pollack, I. B., Santoni, G. W., Schwarz, J. P., Spackman, J. R., Wofsy, S. C., and Parrish, D. D.: Airborne observations of methane emissions from rice cultivation in the Sacramento Valley of California, *J. Geophys. Res.-Atmos.*, 117, Artn D00v25 100 10.1029/2012jd017994, 2012.

Peischl, J., Ryerson, T. B., Brioude, J., Aikin, K. C., Andrews, A. E., Atlas, E., Blake, D., Daube, B. C., de Gouw, J. A., Dlugokencky, E., Frost, G. J., Gentner, D. R., Gilman, J. B., Goldstein, A. H., Harley, R. A., Holloway, J. S., Kofler, J., Kuster, W. C., Lang, P. M., Novelli, P. C., Santoni, G. W., Trainer, M., Wofsy, S. C., and Parrish, D. D.: Quantifying sources of methane using light alkanes in the Los Angeles basin, California, *J. Geophys. Res.-Atmos.*, 118, 4974-4990, 10.1002/jgrd.50413, 2013.

Peischl, J., Eilerman, S. J., Neuman, J. A., Aikin, K. C., de Gouw, J., Gilman, J. B., Herndon, S. C., Nadkarni, R., Trainer, M., Warneke, C., and Ryerson, T. B.: Quantifying Methane and Ethane Emissions to the Atmosphere From Central and Western US Oil and Natural Gas Production Regions, *J. Geophys. Res.-Atmos.*, 110 123, 7725-7740, 10.1029/2018jd028622, 2018.

Pierce, R. B., Al-Saadi, J. A., Schaack, T., Lenzen, A., Zapotocny, T., Johnson, D., Kittaka, C., Bunker, M., Hitchman, M. H., Tripoli, G., Fairlie, T. D., Olson, J. R., Natarajan, M., Crawford, J., Fishman, J., Avery, M., Browell, E. V., Creilson, J., Kondo, Y., and Sandholm, S. T.: Regional Air Quality Modeling System (RAQMS) predictions of the tropospheric ozone budget over east Asia, *J. Geophys. Res.*, 108, 8825, 10.1029/2002jd003176, 2003.

Polvani, L. M., and Esler, J. G.: Transport and mixing of chemical air masses in idealized baroclinic life cycles, *J. Geophys. Res.-Atmos.*, 112, Artn D23102 115 10.1029/2007jd008555, 2007.

|120 Pozzer, A., Schultz, M. G., and Helmig, D.: Impact of US Oil and Natural Gas Emission Increases on Surface Ozone Is Most
Pronounced in the Central United States, *Environmental Science & Technology*, 54, 12423-12433,
10.1021/acs.est.9b06983, 2020.

Reed, R. J., and Nielsen, E. F.: Fronts in the vicinity of the tropopause, *Arch. Meteorol. Geophys. Bioklim.*, 11, 1-17, 1958.

Ryerson, T. B., Andrews, A. E., Angevine, W. M., Bates, T. S., Brock, C. A., Cairns, B., Cohen, R. C., Cooper, O. R., de
|125 Gouw, J. A., Fehsenfeld, F. C., Ferrare, R. A., Fischer, M. L., Flagan, R. C., Goldstein, A. H., Hair, J. W., Hardesty,
R. M., Hostetler, C. A., Jimenez, J. L., Langford, A. O., McCauley, E., McKeen, S. A., Molina, L. T., Nenes, A.,
Oltmans, S. J., Parrish, D. D., Pederson, J. R., Pierce, R. B., Prather, K., Quinn, P. K., Seinfeld, J. H., Senff, C. J.,
|130 Sorooshian, A., Stutz, J., Surratt, J. D., Trainer, M., Volkamer, R., Williams, E. J., and Wofsy, S. C.: The 2010
California Research at the Nexus of Air Quality and Climate Change (CalNex) field study, *J. Geophys. Res.*, 118,
5830-5866, 10.1002/Jgrd.50331, 2013.

Schuepbach, E., Davies, T. D., and Massacand, A. C.: An unusual springtime ozone episode at high elevation in the Swiss
Alps: contributions both from cross-tropopause exchange and from the boundary layer, *Atmos. Environ.*, 33, 1735-
1744, 1999.

Seidel, D. J., Zhang, Y. H., Beljaars, A., Golaz, J. C., Jacobson, A. R., and Medeiros, B.: Climatology of the planetary
|135 boundary layer over the continental United States and Europe, *J. Geophys. Res.*, 117, D17106,
10.1029/2012jd018143, 2012.

Singh, H. B., Cai, C., Kaduwela, A., Weinheimer, A., and Wisthaler, A.: Interactions of fire emissions and urban pollution
over California: Ozone formation and air quality simulations, *Atmospheric Environment*, 56, 45-51, Doi
10.1016/J.Atmosenv.2012.03.046, 2012.

|140 Skerlak, B., Sprenger, M., and Wernli, H.: A global climatology of stratosphere-troposphere exchange using the ERA-
Interim data set from 1979 to 2011, *Atmos. Chem. Phys.*, 14, 913-937, 10.5194/Acp-14-913-2014, 2014.

Skerlak, B., Sprenger, M., Pfahl, S., Tyrlis, E., and Wernli, H.: Tropopause folds in ERA-Interim: Global climatology and
relation to extreme weather events, *J. Geophys. Res.-Atmos.*, 120, 4860-4877, 10.1002/2014JD022787, 2015.

Sprenger, M., and Wernli, H.: A northern hemisphere climatology of cross-tropopause exchange for the ERA15 time period
|145 (1979-1993), *J. Geophys. Res.*, 108, doi:10.1029/2002JD002636, 2003.

Stein, A. F., Draxler, R. R., Rolph, G. D., Stunder, B. J. B., Cohen, M. D., and Ngan, F.: NOAA'S HYSPLIT Atmospheric
Transport and Dispersion Modeling System, *Bull. Amer. Meteor. Soc.*, 96, 2059-2077, 10.1175/Bams-D-14-
00110.1, 2015.

Sterling, C. W., Johnson, B. J., Oltmans, S. J., Smit, H. G. J., Jordan, A. F., Cullis, P. D., Hall, E. G., Thompson, A. M., and
|150 Witte, J. C.: Homogenizing and estimating the uncertainty in NOAA's long-term vertical ozone profile records
measured with the electrochemical concentration cell ozonesonde, *Atmos Meas Tech*, 11, 3661-3687, 10.5194/amt-
11-3661-2018, 2018.

Stewart, J. Q., Whiteman, C. D., Steenburgh, W. J., and Bian, X. D.: A climatological study of thermally driven wind systems of the US Intermountain West, *Bull. Am. Meteorol. Soc.*, 83, 699-708, 10.1175/1520-0477(2002)083<0699:Acstod>2.3.Co; 2, 2002.

155

Stohl, A., Spichtinger-Rakowsky, N., Bonasoni, P., Feldmann, H., Memmesheimer, M., Scheel, H. E., Trickl, T., Hubener, S., Ringer, W., and Mandl, M.: The influence of stratospheric intrusions on alpine ozone concentrations, *Atmos. Environ.*, 34, 1323-1354, 10.1016/S1352-2310(99)00320-9, 2000.

Thorncroft, C. D., Hoskins, B. J., and McIntyre, M. E.: Two paradigms of baroclinic-wave life-cycle behaviour, *Q. J. R. Meteorol. Soc.*, 119, 17-55, 1993.

160

Tian, H. Q., Yang, J., Xu, R. T., Lu, C. Q., Canadell, J. G., Davidson, E. A., Jackson, R. B., Arneth, A., Chang, J. F., Ciais, P., Gerber, S., Ito, A., Joos, F., Lienert, S., Messina, P., Olin, S., Pan, S. F., Peng, C. H., Saikawa, E., Thompson, R. L., Vuichard, N., Winiwarter, W., Zaehle, S., and Zhang, B. W.: Global soil nitrous oxide emissions since the preindustrial era estimated by an ensemble of terrestrial biosphere models: Magnitude, attribution, and uncertainty, *Global Change Biology*, 25, 640-659, 10.1111/gcb.14514, 2019.

165

Tian, H. Q., Xu, R. T., Canadell, J. G., Thompson, R. L., Winiwarter, W., Suntharalingam, P., Davidson, E. A., Ciais, P., Jackson, R. B., Janssens-Maenhout, G., Prather, M. J., Regnier, P., Pan, N. Q., Pan, S. F., Peters, G. P., Shi, H., Tubiello, F. N., Zaehle, S., Zhou, F., Arneth, A., Battaglia, G., Berthet, S., Bopp, L., Bouwman, A. F., Buitenhuis, E. T., Chang, J. F., Chipperfield, M. P., Dangal, S. R. S., Dlugokencky, E., Elkins, J. W., Eyre, B. D., Fu, B. J., Hall, B., Ito, A., Joos, F., Krummel, P. B., Landolfi, A., Laruelle, G. G., Lauerwald, R., Li, W., Lienert, S., Maavara, T., MacLeod, M., Millet, D. B., Olin, S., Patra, P. K., Prinn, R. G., Raymond, P. A., Ruiz, D. J., van der Werf, G. R., Vuichard, N., Wang, J. J., Weiss, R. F., Wells, K. C., Wilson, C., Yang, J., and Yao, Y. Z.: A comprehensive quantification of global nitrous oxide sources and sinks, *Nature*, 586, 248-+, 10.1038/s41586-020-2780-0, 2020.

170

Trickl, T., Vogelmann, H., Giehl, H., Scheel, H. E., Sprenger, M., and Stohl, A.: How stratospheric are deep stratospheric intrusions?, *Atmos. Chem. Phys.*, 14, 9941-9961, 10.5194/acp-14-9941-2014, 2014.

175

Trickl, T., H. Vogelmann, L. Ries, and M. Sprenger (2020), Very high stratospheric influence observed in the free troposphere over the northern Alps - just a local phenomenon? *Atmos. Chem. Phys.*, 20(1), 243-266, doi:10.5194/acp-20-243-2020.

Trousdale, J. F., Conley, S. A., Post, A., and Faloona, I. C.: Observing entrainment mixing, photochemical ozone production, and regional methane emissions by aircraft using a simple mixed-layer framework, *Atmos. Chem. Phys.*, 16, 15433-15450, 10.5194/acp-16-15433-2016, 2016.

180

Uhl, M., and Moore, T.: Western ozone NAAQS implementation and issues: addressing background and transport, EM / Air and Waste Management Association, September, 6, 2018.

Vaughan, G., Price, J. D., and Howells, A.: Transport into the troposphere in a tropopause fold, *Q. J. R. Meteorol. Soc.*, 120, 1085-1103, 1994.

185

Vaughan, G., and Worthington, R. M.: Break-up of a stratospheric streamer observed by MST radar, *Q. J. R. Meteorol. Soc.*, 126, 1751-1769, 2000.

Vaughan, G., O'Connor, F. M., and Wareing, D. P.: Observations of Streamers in the Troposphere and Stratosphere Using Ozone Lidar, *J. Atmos. Chem.*, 38, 295-315, 2001.

Washenfelder, R. A., Wagner, N. L., Dube, W. P., and Brown, S. S.: Measurement of Atmospheric Ozone by Cavity Ring-down Spectroscopy, *Environmental Science & Technology*, 45, 2938-2944, 10.1021/es103340u, 2011.

Wernli, H.: A Lagrangian-based analysis of extratropical cyclones. II: a detailed case-study, *Q. J. R. Meteorol. Soc.*, 123, 1677-1706, 1997.

Wernli, H., and Bourqui, M.: A Lagrangian "1-year climatology" of (deep) cross-tropopause exchange in the extratropical Northern Hemisphere, *J. Geophys. Res.*, 107, 10.1029/2001JD000812, 2002.

Wild, R. J., Edwards, P. M., Dube, W. P., Baumann, K., Edgerton, E. S., Quinn, P. K., Roberts, J. M., Rollins, A. W., Veres, P. R., Warneke, C., Williams, E. J., Yuan, B., and Brown, S. S.: A Measurement of Total Reactive Nitrogen, NO_y, together with NO₂, NO, and O₃ via Cavity Ring-down Spectroscopy, *Environmental Science & Technology*, 48, 9609-9615, 10.1021/es501896w, 2014.

Wild, R. J., Dube, W. P., Aikin, K. C., Eilerman, S. J., Neuman, J. A., Peischl, J., Ryerson, T. B., and Brown, S. S.: On-road measurements of vehicle NO₂/NO_x emission ratios in Denver, Colorado, USA, *Atmospheric Environment*, 148, 182-189, 10.1016/j.atmosenv.2016.10.039, 2017.

Wirth, V., Appenzeller, C., and Juckes, M.: Signatures of induced vertical air motion accompanying quasi-horizontal roll-up of stratospheric intrusions, *Mon. Wea. Rev.*, 125, 2504-2519, 1997.

Womack, C. C., Neuman, J. A., Veres, P. R., Eilerman, S. J., Brock, C. A., Decker, Z. C. J., Zarzana, K. J., Dube, W. P., Wild, R. J., Wooldridge, P. J., Cohen, R. C., and Brown, S. S.: Evaluation of the accuracy of thermal dissociation CRDS and LIF techniques for atmospheric measurement of reactive nitrogen species, *Atmos Meas Tech*, 10, 1911-1926, 10.5194/amt-10-1911-2017, 2017.

Xiao, Y., Jacob, D. J., Wang, J. S., Logan, J. A., Palmer, P. I., Suntharalingam, P., Yantosca, R. M., Sachse, G. W., Blake, D. R., and Streets, D. G.: Constraints on Asian and European sources of methane from CH₄-C₂H₆-CO correlations in Asian outflow, *Journal of Geophysical Research: Atmospheres*, 109, <https://doi.org/10.1029/2003JD004475>, 2004.

Zhang, L., D. J. Jacob, N. V. Downey, D. A. Wood, D. Blewitt, C. C. Carouge, A. van Donkelaar, D. B. A. Jones, L. T. Murray, and Y. X. Wang (2011), Improved estimate of the policy-relevant background ozone in the United States using the GEOS-Chem global model with 1/2 degrees x 2/3 degrees horizontal resolution over North America, *Atmos. Environ.*, 45(37), 6769-6776, doi:10.1016/J.Atmosenv.2011.07.054.

Zhang, L., Lin, M. Y., Langford, A. O., Horowitz, L. W., Senff, C. J., Klovinski, E., Wang, Y. X., Alvarez, R. J., Petropavlovskikh, I., Cullis, P., Sterling, C. W., Peischl, J., Ryerson, T. B., Brown, S. S., Decker, Z. C. J., Kirgis, G., and Conley, S.: Characterizing sources of high surface ozone events in the southwestern US with intensive field measurements and two global models, *Atmospheric Chemistry and Physics*, 20, 10379-10400, 10.5194/acp-20-10379-2020, 2020.

1220